

# 1996/1997 LOW LUMINOSITY STATE AND STATE TRANSITIONS OF GRS 1915+105: RXTE OBSERVATIONS

S. Trudolyubov<sup>1,2</sup>, E. Churazov<sup>1,2</sup>, M. Gilfanov<sup>1,2</sup>

<sup>1</sup> *Space Research Institute, Russian Academy of Sciences,  
Moscow, Russia*

<sup>2</sup> *Max-Planck-Institut für Astrophysik, Garching bei München,  
Germany*

## ABSTRACT

The results of X-ray observations of Galactic superluminal jet source GRS 1915+105 during its low luminosity state and state transitions in October, 1996 – April, 1997 with *PCA* and *HEXTE* instruments aboard *Rossi X-ray Timing Explorer (RXTE)* are reported.

Except some peculiarities, the major spectral and temporal properties of the source during this period were similar to that of the Galactic black hole candidates in the *intermediate* state (corresponding to the transition between the canonical *high* and *low* states). The power law component of the spectrum gradually hardens with decrease of the source flux in the 3 – 150 keV energy band. The 2 – 10 Hz QPOs were found to be a generic feature of the power density spectrum in this state. *The changes of the QPO centroid frequency are strongly correlated with the changes of spectral and timing parameters (in particular parameters of the soft spectral component). This type of correlation holds on the wide range of time scales (from ~ seconds to ~ months).* Overall trend of the spectral and temporal properties suggests that with further drop of the source flux (below the values observed during the reported period) they would match the canonical values for a *low* state of the Galactic black hole candidates.

## Introduction

The X-ray source GRS 1915+105, one of two Galactic objects which show the superluminal expansion of matter, was discovered by *GRANAT* observatory as a transient in 1992 (Castro-Tirado, Brandt & Lund 1992). Radio observations of superluminal motion have allowed to determine the distance ( $\sim 12.5$  kpc) and inclination of the system (Mirabel & Rodriguez 1994). The source is believed to be a black hole candidate on the basis of its observed high luminosity exceeding the Eddington limit (Sazonov *et al.* 1994) for a neutron star and similarities to another Galactic superluminal jet source GRO J1655-40 (Zhang *et al.* 1994), whose dynamical mass estimate ( $\sim 7M_{\odot}$ ) implies the presence of a black hole (Orosz & Bailyn 1997). Long-term temporal behavior of GRS 1915+105 is very complicated: since the discovery a number of outbursts and low luminosity episodes have been reported (Sazonov *et al.* 1996; Pacieras *et al.* 1996).

Since April, 1996 GRS 1915+105 is a target of the *RXTE* TOO regular observations, which have revealed rich character of the source transient activity including the occasional complicated patterns of dips, flares and rapid transitions between high and low intensity alternated with the relatively quiet periods and also strong quasi-periodic oscillations (Greiner, Morgan & Remillard 1996; Chen *et al.* 1997; Belloni *et al.* 1997*b*; Morgan *et al.* 1997).

We have performed the systematic study of the evolution of GRS 1915+105 properties using the data of PCA and HEXTE instruments aboard *RXTE* **i**) to resolve the mutual dependence of the spectral and timing parameters of the source emission and **ii**) to understand how the low luminosity state of GRS 1915+105 observed in October, 1996 – April, 1997 fits the standard scheme of the 'canonical' *high/low* states established for Galactic black hole candidates (Tanaka & Lewin 1995).

In this paper we report the results of the GRS 1915+105 *RXTE* observations during its low luminosity state and state transitions in October, 1996 – April, 1997. The discussion of implications of these data on to the physical models will be presented in the subsequent paper (Trudolyubov *et al.* 1998).

## Instruments and observations

The observations discussed below were performed with the Proportional Counter Array (PCA) and the High Energy Timing Experiment (HEXTE)

aboard *Rossi X-ray Timing Explorer (RXTE)* (Bradt, Swank, & Rotshild 1993) in October, 1996 – April, 1997. The list of observations is presented in Table 1.

For the processing of the PCA data we used standard *RXTE* FTOOLS version 4.1 tasks. For the background subtraction the version of the background estimator program taking into account the effects of activation due to the South Atlantic Anomaly, X-ray background and particle background based on the measurements of the Q6 rate (Stark 1997) was used.

For the spectral analysis of the PCA data we used the 3.2.1 version of the response matrix. In order to account for the uncertainties of the response matrix, a 1%– systematic error was added to the statistical error for each PCA energy channel. We have excluded from the spectral analysis the data below 3 keV because of the rapid drop of the PCA effective area in this energy domain. In addition, because of the strong influence of the response uncertainties at high energies, the data above 20 keV were also ignored. To evaluate the correct source flux, the standard dead–time correction procedure (Zhang & Jahoda 1996) was applied to the PCA data.

HEXTE data also have been processed using the standard FTOOLS version 4.1 tasks. We used latest available HEXTE response matrices, released on April 3, 1997 and standard off–source observations for each cluster of detectors to subtract background. In order to account for the uncertainties in the response and background determination, only data in the 20 – 150 keV energy range were taken for the spectral analysis.

## Results

The *RXTE*/ASM light curve of the GRS 1915+105 in the 2 – 12 keV energy band is shown in figure 1. Prior to the end of October, 1996 (MJD  $\sim$  50386) the source was in the bright highly variable so called 'chaotic' state with average flux  $\sim$  1 Crab (Morgan *et al.* 1997) and then has underwent transition to the low luminosity state (LLS) lasting  $\sim$  200 days. The corresponding X-ray luminosity of the source dropped from  $\sim 10^{39} \text{erg/s}$  to  $\sim 2 \times 10^{38} \text{erg/s}$  in the 3 – 20 keV energy band (assuming the distance of 12.5 kpc). After the April 25, 1997 (MJD 50564) GRS 1915+105 appeared to return to the high luminosity state (HLS). Contrary to the HLS with its high level of variability, the evolution of the source flux during LLS can be described as a relatively smooth decline to the  $\sim$  200 – 250 mCrab level during first  $\sim$  100 days

followed by the similar–fashioned slow rise on the similar time scale.

We present below the basic results of the systematic spectral and timing analysis of the source emission during the low luminosity state and state transitions using the data of PCA and HEXTE observations (Table 1).

## Spectral analysis

As we are interested in the general character of the GRS 1915+105 spectral evolution, we used only simplest models (a sum of a multicolor disk black body model <sup>1</sup> and a power law model with exponential cutoff corrected for the interstellar absorption) to approximate its energy spectrum. Although this model provides satisfactory description to the overall shape of the spectrum, there is a significant excess of emission in the 6 – 8 keV region (with an average ratio of excess to the model continuum of  $\sim 2 - 3\%$ ), which is attributed to the presence of the iron emission/absorption complex. Due to the relatively low energy resolution of the PCA instrument ( $\Delta E \sim 1$  keV in the 6 – 8 keV range) it is not possible to carry out a detailed analysis of this spectral feature. The presence of the iron emission/ absorption features shows the evidence for the additional 'reprocessed' component in the source spectrum, but its approximation by certain type of model requires further physical justification, so we have decided not to include 'reprocessed' component to the fit. <sup>2</sup> Because of the large uncertainty in the PCA response in the low energy domain, we fixed the equivalent hydrogen column density in the spectral fitting at the value of  $\sim 5.0 \times 10^{22} \text{cm}^{-2}$ , determined from ASCA observations (Ebisawa *et al.* , 1995). Due to the present difference in the relative normalizations of the PCA and HEXTE spectra, we used PCA normalization to compute broad-band spectral model fluxes.

We have generated the energy spectra of the source averaging the data over the whole observations. To trace the evolution of the spectral parameters during the individual observations with relatively high level of X-ray flux variability, additional analysis of the spectra, accumulated in the 16 – 80 s

---

<sup>1</sup>Note that no corrections for the electron scattering and effects of general relativity were made (Shakura & Sunyaev, 1973, Shimura & Takahara 1995), T is a measured color temperature

<sup>2</sup>See Greiner *et al.* 1998 for the results of fitting of GRS 1915+105 LLS spectra with inclusion of the Compton reflection model

time intervals, has been performed<sup>3</sup>. This procedure has allowed us to study the evolution of the main spectral parameters of GRS 1915+105 in a wide range of time scales from *tens of seconds* to *months*.

For comparison with the low luminosity state (LLS) observations, we have analyzed the data for several observations of GRS 1915+105 covering the period of high luminosity state (HLS) (October 7,13,15 1996 observations) occurred just prior to the transition to the LLS. The typical broad-band spectra of the GRS 1915+105 in the HLS (in units of  $F(E) \times E^2$ ) are shown in Figure 2 (*left panel*). The source exhibits extremely complicated pattern of the spectral variability on the different time scales (Belloni *et al.* 1997*a*, Belloni *et al.* 1997*b*, Taam *et al.* 1997). The most striking feature of the spectral variation is the existence of two distinct types of broad-band spectrum corresponding to the highest ('flare') and lowest ('quiescence') levels of source luminosity (Figure 2). The energy spectrum in the 3 – 150 keV energy range can be well represented as a composition of the soft and hard components (Figure 2). The form of the hard spectral component in general is described by a power law (photon index  $\alpha \sim 2.0 - 2.6$ ) which becomes steeper ( $\alpha \sim 3.0 - 3.5$ ) at around  $\sim 25 - 30$  keV. During the 'flare' the slope of the high energy part of the spectrum is  $\sim 3.0 - 3.5$ . The measured color temperature of the soft component is noted to be higher in the 'flare' state (see Belloni *et al.* 1997*b*).

Since October 23, 1996 GRS 1915+105 has begun a transition to the low luminosity state lasting till November 28. During this time the source shows a rich character of the spectral variability alternating relatively quiet periods of low X-ray flux with a bright flaring episodes. As an example of the short-term spectral variability of GRS 1915+105 during the transition to the LLS the evolution of the basic spectral parameters of the source for the November 7, 1996 observation is shown in Figure 3. It is clearly seen that the changes of the X-ray flux are connected with the significant change in the slope of the high energy part of the spectrum and large variations of the soft component parameters. The hardness of the high energy part of the source spectrum expressed in terms of the best fit power law model parameters is closely related to the total X-ray flux (Figure 4, 5; 3). In addition, when the luminosity of the source is low enough, the cutoff of the spectrum becomes detectable with HEXTE at the energies of  $\sim 70 - 120$  keV (Figure 5).

---

<sup>3</sup>Only PCA data were used for the analysis because of the insufficient statistical significance of the HEXTE spectral data accumulated during these time intervals

The broad-band 3–150 keV energy spectrum of GRS 1915+105 in the low luminosity state is also satisfactorily described by the sum of two components: relatively weak soft thermal component with a characteristic temperature  $kT \sim 1.0 - 1.7$  keV) and strong hard component which has approximately power law form ( $\alpha \sim 1.8 - 2.4$ ) in the 20 – 60 keV interval and cut-offs at around  $\sim 70 - 120$  keV (Figure 2, *right panel*).

The results of fitting of the HEXTE data with a power law model and PCA data with a composition of a power law and multicolor disk black body model for the observations covering the period from October 7, 1996 to April 25, 1997 (state transitions and low luminosity state) presented in figures 4 and 5 respectively. There is a strong correlation of the slope of high energy part of the spectrum and the source X-ray flux (Figure 6).

## Timing analysis

To perform the analysis of the GRS 1915+105 timing properties we generated power density spectra in the 0.01 – 50 Hz frequency range for two energy bands (2 – 13 and 13 – 60 keV) using short stretches of data. For the observations with a high variability separate power density spectra were produced for the parts of observation divided according to the level of the source flux. The resulting spectra were logarithmically rebinned when necessary to reduce scatter at high frequencies. The power density spectra were normalized to squared fractional *rms*. The white-noise level due to Poissonian statistics corrected for the dead-time effects was subtracted.

To study the evolution of the basic timing parameters of GRS 1915+105 within the individual observations with a relatively high level of variability we generated power density spectra of the source accumulated in the 16 – 80 s time intervals according to the procedure described above.

Typical broad-band power density spectra of GRS 1915+105 during high luminosity 'flaring' state (HLS) prior to Oct. 23, 1996, transition from the HLS to low luminosity state (LLS) and LLS are shown in Figure 7. For the 'flaring' state two spectra corresponding to the highest ('flare') and lowest ('quiescence') levels of source luminosity are displayed (Figure 7, *top left panel*).

The character of PDS evolution during the source state transitions between October 23 and November 28 is very complicated. Fast changes in the form of the power spectrum, correlated with spectral and luminosity changes

on the various time scales (from  $\sim$  several hours to  $\sim$  week) were detected (Figure 7, *right upper, left lower panel*). In spite of drastic differences in the form of the broad-band continuum, relatively narrow QPO peak at frequencies  $\sim 2 - 10$  Hz has been found to be common for all observations covering this period. Basing on the results of the time-resolved PDS analysis of the individual observations with a high level of flux variability, the correlation between the value of the QPO centroid frequency and total X-ray flux and a bolometric flux of the soft spectral component was established (Figure 8).

Beginning on November 28, when the source reached the low luminosity state, the form of the power density spectrum is nearly flat between 0.1 and 1.0 Hz, changing its slope to a value of  $\sim -(1.0 - 2.5)$  in the 1 – 15 Hz and  $\sim 2.0 - 3.0$  in the 15 – 50 Hz range. For some observations the power density spectrum shows a notable rise (sometimes the extra component is flat-topped or has a power law form) towards lower frequencies between 0.01 and 1.0 Hz. The most outstanding features in the GRS 1915+105 power density spectrum are the strong, relatively narrow ( $\Delta f/f \sim 0.1 - 0.3$ ) QPOs placed near the breakpoint in the slope of the broad-band continuum. These QPOs were noted for showing harmonics with a strength that decreases with increasing of the QPO centroid frequency. Positive correlation between the QPO centroid frequency and total X-ray luminosity of the source on the  $\sim$  several hours time scale was detected again (Figure 8), however this type of correlation breaks on the longer time scales.

We fitted the power density spectra in the 0.05 – 50 Hz frequency range to analytic model using  $\chi^2$  minimization technique to trace the evolution of their main parameters with time during transitions and low luminosity state. The data of Oct., 10, 13, 15, 25 and Nov., 19 were excluded from the analysis because of the complicated shape of the PDS caused by the existence of several distinct types of the PDS due to extremely high level of source variability during these observations.

## Analytic approximation

To approximate the broad-band PDS continuum and quantify its characteristics, we used the sum of up to three band-limited noise components, expressed with flat-topped broken power law functions, i. e.:

$$P(f) = \begin{cases} A, & f < f^{br}; \\ A(f/f^{br})^{-\alpha}, & f > f^{br}, \end{cases}$$



where  $f_{br}$  is a BLN characteristic break frequency; and in some cases add a power law (PL) component:

$$P(f) = Bf^{-\alpha},$$

where  $A$  and  $B$  are in units of  $(rms/mean)^2$ . Up to four Lorentzian peaks were used to model a QPO features. In Figure 9 the schematic presentation of the model is shown. Simple fits with the Lorentzian shapes have shown that regardless of the continuum model type centroid frequencies and widths of the QPO peaks are harmonically related. Taking this fact into account in order to reduce the total number of model parameters we fixed centroid frequencies and widths of QPO components to harmonic ratios.

The best-fit values of the model parameters are summarized in Tables 3, 4 and 5, 6. Parameter errors and upper limits correspond to  $1\sigma$  and  $2\sigma$  confidence levels respectively. This model approximates the data reasonably well, as indicated by the values of reduced  $\chi^2$  of the fit.

## Correlations between timing parameters

In order to summarize the results of analysis of the source power density spectra during the low luminosity state and state transitions, the main best-fit parameters of the PDS are shown as a functions of the fundamental QPO peak frequency for the soft (2 – 13 keV) and hard (13 – 60 keV) energy bands (Figure 10, 11). (*Open circles* correspond to the observations covering the transition from the high luminosity state (HLS) to the low luminosity state (LLS) prior to Nov. 28, 1996 (MJD 50415); *solid circles* correspond to the period of LLS (Dec. 1996 – Apr. 1997)).

*Soft energy band (2 - 13 keV)* As it is clearly seen from Figure 10, the QPO centroid frequency is strongly anticorrelated with the value of the total fractional *rms* (except for the cases when the contribution of the power law (PL) noise component to the total variability is noticeable, which is probably due to presence of the prominent soft component in the energy spectrum (Nov., 7 and Apr., 2 observations)) and with the *rms* of the band-limited noise. The same tendency is hold for the value of fractional *rms* of the fundamental QPO peak: it decreases with the increase of the QPO frequency. In addition, there is a close relation between the positions of the QPO peaks and characteristic breaks in the BLN continuum (Figure 10, *top panels*).

*Hard energy band (13 - 60 keV)* Most of the correlations, noted for the soft energy band are also observed for the data in the hard band, except for the total *rms* and BLN *rms*, which do not show any correlation with the

QPO centroid frequency (Figure 11).

## Correlations between spectral and timing parameters

We have analyzed the relation between the spectral and temporal properties of GRS 1915+105. During the low luminosity state and state transitions the change of the QPO centroid frequency is correlated with the change of the spectral parameters, derived using our simplified spectral model. In figure 12 the relationship between the total fractional *rms* integrated over 0.05 – 50 Hz frequency range and X-ray flux (3 – 20 keV) for the soft (2 – 13 keV) and hard (13 – 60 keV) energy bands is presented. As the contribution of the soft spectral component to the 13 – 60 keV flux is small, we can examine the properties of the hard spectral component alone using variability analysis of the data in this range. As it is seen from figure 12, the level of the band-limited noise continuum *rms* in the 13 – 60 keV energy domain is strongly correlated with the total X-ray flux and, in particular, with the hard spectral component flux (Figure 13), which makes a main contribution to the total X-ray flux. *There is a clear trend of rising the QPO frequency with the rise of the soft component flux (Figure 14). It should be noted that this type of correlation holds on the wide range of time scales (from  $\sim$  seconds to  $\sim$  months).* Further discussion of the frequency/spectrum correlations are presented in Trudolyubov *et al.* 1998.

## Summary

We have presented the results of the RXTE observations of the GRS 1915+105 during its low luminosity state in November, 1996 – April, 1997.

This period is characterized by the drop of the source flux in the standard X-ray band by a factor of  $\sim 2 - 5$  with respect to the bright flaring state (Figure 1). Contrary to the high luminosity state (HLS) with its high level of variability, the evolution of the source flux during low luminosity state can be described as a relatively smooth decline to the lowest level during first  $\sim 100$  days followed by similar-fashioned slow rise on the same time scale.

The broad-band X-ray spectrum of GRS 1915+105 can be generally described by composition of the soft component and an extended high energy tail (Figure 2, *right panel*). In order to characterize the general character of the source spectral evolution we used a composition of the multicolor disk

blackbody model and a power law model with exponential cut-off. The contribution of the soft component, dominating the source luminosity in the HLS prior to transition, dropped to  $< 25\%$  in the 3 – 20 keV energy band. In general the evolution of GRS 1915+105 broad-band spectrum during low luminosity state and state transitions can be characterized by the decrease of the soft component flux accompanied by gradual flattening of the hard spectral component with decrease of the total source intensity, followed by rise of the soft component flux and hard component steepening as the overall source luminosity become increasing again.

The temporal properties of GRS 1915+105 during LLS were also quite different from those in the HLS. The overall shape of the source power density spectrum in the 0.01 – 50 Hz frequency is roughly presented by the composition of the flat-topped band-limited (BLN) and a power law (PL) noise components. Strong, relatively narrow ( $\delta f/f \sim 0.2$ ) QPOs with a centroid frequency at about 2 – 10 Hz located near the break of the BLN continuum slope is found to be a generic feature of the GRS 1915+105 power density spectrum. In addition, the QPO peaks are noted for showing harmonic content. Close relation between the main parameters describing the power density spectrum of the source (QPO centroid frequency, characteristic BLN break frequency, broad-band *rms*) may hint on the general character of the band-limited noise and QPO production.

*The most striking is the established close relation between the evolution of the spectral and timing parameters of the source. The change of the QPO centroid frequency is correlated with the change of the spectral parameters, derived using our simplified spectral model. In particular, there is a clear trend of rising the QPO frequency with the rise of the soft component flux (Figure 14). It should be noted that this type of correlation holds on the wide range of time scales (from  $\sim$  seconds to  $\sim$  months).*

The complex of GRS 1915+105 X-ray properties is very similar to that of some Galactic black hole candidates observed in the so-called 'intermediate' state during their *high-to-low* and *low-to-high* state transitions (Cygnus X-1 (Belloni *et al.* 1996, Cui *et al.* 1997); GX 339-4 (Mendez & Van der Klis 1996); GS 1124-68 (Miyamoto *et al.* 1994, Takizawa *et al.* 1996); GRO J1655-44 (Mendez *et al.* 1998)). In fact, there are several general properties of GRS 1915+105 showing that this state of the source does not match neither 'canonical' *low* nor *high* state and probably corresponds to the transition between these states:

1) the overall X-ray luminosity in the low luminosity state  $L_{LLS} \sim 2 \times$

$10^{38} \text{ erg/s}$  is sufficiently lower than in the high luminosity state  $L_{HLS} > 10^{39} \text{ erg/s}$ , which was observed earlier and had the properties typical for the *high* state;

2) contrary to the typical *low* state energy spectrum of the source shows clear evidence for the soft component, but its contribution to the total X-ray luminosity is small ( $< 30\%$ ) instead of  $\sim 70 - 90\%$  in the case of *high* state;

3) the power density spectrum also differs from the typical power density spectra in the *low* and *high* states: contrary to the 'canonical' *soft* state it shows the presence of the prominent band-limited noise component, while the frequency of the characteristic peak of the BLN continuum ( $\sim 2 - 10 \text{ Hz}$ ) is one order of magnitude higher than usually expected for the typical low state of Galactic black hole candidates.

Basing on the results of *RXTE* observations we can conclude that during this low luminosity episode inspite of some peculiarities, the major X-ray properties of GRS 1915+105 were similar to that of Galactic black hole candidates in the *transition* or 'intermediate' state. The observed trends of hardening the energy spectra, rise of the BLN *rms*, decrease of the QPO frequency with the decrease of the source luminosity seem to suggest that further decrease of the luminosity (below the values observed during November, 1996 – April, 1997) would put the source to the canonical low state established for the Galactic black hole candidates. It is likely that the source was observed in the 'intermediate' state simply because the luminosity (mass accretion rate) did not drop sufficiently enough for the source to reach canonical *low/hard* state.

This research has made use of data obtained through the High Energy Astrophysics Science Archive Research Center Online Service, provided by the NASA/Goddard Space Flight Center.

This work was supported in part by the grants RBRF grant 96-02-18588 and INTAS grant 93-3364-ext. S. Trudolyubov was partially supported by grant of the International Science Foundation.

## References

- Belloni, T., Mendez, M., Van der Klis, M., Hasinger, G., Lewin, W. H. G., & Van Paradijs, J. 1996, *ApJ*, 472, L107
- Belloni, T., van der Klis, M., Lewin, W. H. G., Van Paradijs, J., Dotani, T., Mitsuda, K., Miyamoto, S. 1997, *A&A*, 322, 857
- Belloni, T., Mendez, M., King, A. R., Van der Klis, M., & Van Paradijs, J. 1997*a*,

ApJ, 479, L145  
Belloni, T., Mendez, M., King, A. R., Van der Klis, M., & Van Paradijs, J. 1997*b*,  
ApJ, 488, L109  
Bradt, H., Swank, J., & Rothschild, R. 1993, A&AS, 97,355  
Chen, X., Swank, J. H., & Taam, R. E. 1997, ApJ, 477, L41  
Cui, W., Zhang, S. N., Focke, W., & Swank, J. H. 1997, ApJ, 484, 383  
Ebisawa, K., White, N. E., & Kotani, T. 1995, IAU Circ. 6171  
Greiner, J., Morgan, E. H., & Remillard, R. A. 1998, astro-ph/9806323  
Jahoda, K. 1997,  
<http://lheawww.gsfc.nasa.gov/users/keith/pcarmf.html>  
Mendez, M., & Van der Klis, M. 1996, ApJ, 479, 926  
Mendez, M., Belloni, T., & Van der Klis, M. 1998, ApJ, 489, L187  
Mirabel, I. F., & Rodriguez, L. F. 1994, Nature, 371, 46  
Miyamoto, S., Kitamoto, S., Iga, S., Hayashida, K., Terada, K. 1994, ApJ, 435,  
389  
Mitsuda, K. *et al.* 1984, PASJ, 36, 741  
Morgan, E. H., Remillard, R. A., & Greiner, J. 1997, ApJ, 482, 993  
Paciesas, W. S., Deal, K. J., Harmon, B. A., Zhang, S. N., Wilson, C. A., & Fish-  
man, G. J. 1996, A&AS, 120, 205  
Remillard, R. A., & Morgan, E. H. 1998, astro-ph/9805237  
Sazonov, S., Sunyaev, R., Alexandrovich, N., & Borozdin, K. 1994, IAU Circ. 6080  
Sazonov, S., Sunyaev, R., & Lund, N. 1996, in Proc. of X-ray Conference, eds.  
Zimmermann, H.U., Truemper, J., & Yorke, H. (MPE Report 263), 187  
Shakura, N. I., & Sunyaev, R. A. 1973, A&A, 24, 337  
Shimura, T., & Takahara, F. 1995, ApJ, 445, 780  
Stark 1997,  
<http://lheawww.gsfc.nasa.gov/users/stark/pca/pcabackest.html>  
Taam, R. E., Chen, X., Swank, J. H. 1997, ApJ, 485, L83  
Takizawa, M., Dotani, T., Mitsuda, K., Matsuba, E., Ogawa, M., Aoki, T., Asai,  
K., Ebisawa, K., Makishima, K., Miyamoto, S., Iga, S., Vaughan, B., Rutledge,  
R., & Lewin, W. H. G. 1996, ApJ, 489, 272  
Tanaka, Y., & Lewin, W. H. G. 1995, in X-ray Binaries, ed. W. H. G. Lewin, J.  
Van Paradijs, & E. P. J. van den Heuvel (Cambridge: Cambridge Univ. Press),  
126  
Trudolyubov, S. *et al.* (in preparation)  
Zhang, W., & Jahoda, K. 1996,  
<http://lheawww.gsfc.nasa.gov/users/keith/deadtime/deadtime.html>  
Zhang, W., Jahoda, K., Swank, J. H., Morgan, E. H., & Giles, A. B. 1995, ApJ,

449, 930

Table 1: *RXTE* observations of GRS 1915+105 in October, 1996 – May, 1997.

MJD	Date, UT	Time, UT (h:m:s)	Exposure <sup>a</sup> , s		
			PCA	HEXTE–A	HEXTE–B
50363	07/10/1996	05 : 44 : 36 – 11 : 11 : 13	10944	1252	1100
50369	13/10/1996	10 : 03 : 17 – 14 : 06 : 13	7756	1165	1156
50371	15/10/1996	15 : 10 : 39 – 22 : 30 : 13	7856	1274	1253
50379	23/10/1996	11 : 53 : 56 – 18 : 25 : 13	9072	1289	1261
50381	25/10/1996	11 : 52 : 51 – 17 : 44 : 13	7216	1327	1288
50385	29/10/1996	11 : 53 : 13 – 17 : 29 : 14	5116	2700	2717
50394	07/11/1996	05 : 42 : 38 – 09 : 07 : 14	7760	2084	2131
50401	14/11/1996	02 : 17 : 24 – 03 : 42 : 13	2944	888	895
50406	19/11/1996	02 : 52 : 20 – 07 : 39 : 13	6368	3890	1285
50415	28/11/1996	03 : 04 : 13 – 06 : 16 : 13	6969	1275	817
50421	04/12/1996	23 : 25 : 58 – 03 : 26 : 13	1952	1130	1120
50428	11/12/1996	18 : 42 : 12 – 22 : 42 : 14	9232	2339	2340
50436	19/12/1996	15 : 47 : 20 – 19 : 47 : 13	8623	2430	2510
50441	24/12/1996	22 : 04 : 38 – 01 : 28 : 13	5888	1939	1978
50448	31/12/1996	06 : 48 : 53 – 10 : 19 : 13	7284	1353	1349
50455	07/01/1997	23 : 50 : 28 – 04 : 08 : 13	3215	2569	2676
50462	14/01/1997	01 : 29 : 43 – 03 : 59 : 14	6250	1275	1314
50471	23/01/1997	01 : 39 : 50 – 05 : 51 : 14	9016	2287	2342
50477	29/01/1997	20 : 57 : 32 – 01 : 38 : 13	9563	2045	1086
50480	01/02/1997	21 : 08 : 59 – 01 : 37 : 13	9010	2788	2796
50488	09/02/1997	18 : 41 : 59 – 00 : 01 : 13	9847	2483	2515
50501	22/02/1997	21 : 14 : 51 – 23 : 36 : 13	5739	1865	1854
50512	05/03/1997	21 : 20 : 31 – 22 : 55 : 13	4564	1792	1801
50517	10/03/1997	01 : 07 : 20 – 04 : 27 : 13	5648	1890	1891
50524	17/03/1997	22 : 10 : 05 – 01 : 55 : 13	7824	3921	3916
50534	27/03/1997	21 : 43 : 35 – 23 : 14 : 13	3264	990	974
50540	02/04/1997	12 : 35 : 28 – 14 : 14 : 13	3300	988	996
50557	19/04/1997	10 : 41 : 03 – 14 : 50 : 13	2368	2181	2086
50561	23/04/1997	03 : 08 : 24 – 05 : 19 : 13	3520	1093	1064
50563	25/04/1997	14 : 03 : 56 – 20 : 56 : 14	13105	3467	2481

<sup>a</sup> – dead time corrected value of used exposure time

Table 2: The evolution of the X-ray flux and the level of the short-term variability of GRS 1915+105 during the low luminosity state and state transitions in October, 1996 – April, 1997. For observations with a high level of variability the ranges of parameter change are displayed.

MJD	Date, UT	X-ray Flux*	RMS Intensity	RMS Intensity
		$F_{3-20}, \times 10^{-8}$ ( $erg\ s^{-1}\ cm^{-2}$ )	Variation (%) <sup>1</sup>	Variation (%) <sup>2</sup>
50379	23/10/1996	3.538 – 4.650	15.2 – 17.7	26.0 – 27.6
50385	29/10/1996	1.967 – 2.182	20.3 – 21.4	31.8 ± 2.0
50394	07/11/1996	2.111 – 5.427	15.6 – 17.6	24.2 – 28.9
50401	14/11/1996	3.523	17.2 ± 0.1	27.2 ± 0.2
50406	19/11/1996	3.407	33.4 ± 0.3	25.7 ± 0.2
50415	28/11/1996	1.932 – 3.084	16.2 – 17.8	25.1 – 27.1
50421	04/12/1996	1.820	23.6 ± 0.1	29.8 ± 0.1
50428	11/12/1996	1.553 – 1.685	21.7 – 24.6	27.4 – 29.0
50436	19/12/1996	1.669	22.1 – 24.1	27.7 – 29.1
50441	24/12/1996	1.656	19.1 ± 0.1	25.4 ± 0.1
50448	31/12/1996	1.398	23.5 ± 0.3	26.7 ± 0.2
50455	07/01/1997	1.263	22.2 – 23.3	25.1 – 25.9
50462	14/01/1997	1.155	22.5 ± 0.1	24.7 ± 0.1
50471	23/01/1997	1.131	23.1 ± 0.1	24.8 ± 0.1
50477	29/01/1997	1.183	21.0 ± 0.1	24.4 ± 0.1
50480	01/02/1997	1.148	20.9 ± 0.3	24.2 ± 0.2
50488	09/02/1997	1.049	24.7 ± 0.1	24.5 ± 0.1
50501	22/02/1997	1.012	22.6 ± 0.1	23.1 ± 0.1
50512	05/03/1997	1.067	21.8 ± 0.1	23.6 ± 0.2
50517	10/03/1997	0.978	25.5 ± 0.3	24.5 ± 0.2
50524	17/03/1997	1.020	22.0 ± 0.1	23.4 ± 0.1
50534	27/03/1997	1.002	20.2 ± 0.1	22.8 ± 0.2
50540	02/04/1997	1.114	19.5 ± 0.4	23.2 ± 0.2
50548	10/04/1997	1.102	18.1 ± 0.2	21.3 ± 0.2
50561	23/04/1997	1.216	23.4 ± 0.1	25.0 ± 0.1
50563	25/04/1997	1.340 – 1.413	17.0 – 19.0	22.1 – 23.3

\* – value, corrected for interstellar absorption

<sup>1</sup> – 2 – 13 keV energy band, 0.05 – 50 Hz frequency range

<sup>2</sup> – 13 – 60 keV energy band, 0.05 – 50 Hz frequency range



Table 3: The characteristics of the power density spectrum. Parameter errors and upper limits correspond to the  $1\sigma$  and  $2\sigma$  confidence levels respectively.  $rms_{BLN}$  represents the total  $rms$  of the band-limited components integrated in the 0.05 – 50 Hz frequency range. Observations with sufficiently high level of variability are presented by several subsets of data.

Energy (keV)	$f_1^{br}$ (Hz)	$\alpha_1$	$f_2^{br}$ (Hz)	$\alpha_2$	$f_3^{br}$ (Hz)	$\alpha_3$	$rms_{BLN}$ (%)
<i>23/10/1996</i>							
2 – 13	$0.51^{+0.03}_{-0.08}$	$2.20^{+0.31}_{-0.34}$	$2.58^{+0.03}_{-0.03}$	$5.50^{+0.50}_{-1.23}$	$10.29^{+0.10}_{-0.07}$	$3.10^{+0.09}_{-0.06}$	$14.1^{+0.6}_{-0.5}$
13 – 60	$0.66^{+0.04}_{-0.05}$	$2.92^{+0.55}_{-0.60}$	$2.05^{+0.03}_{-0.03}$	$4.32^{+0.42}_{-0.37}$	$6.79^{+0.17}_{-0.16}$	$2.27^{+0.09}_{-0.08}$	$23.8^{+0.9}_{-0.9}$
2 – 13	$0.58^{+0.02}_{-0.02}$	$2.24^{+0.36}_{-0.13}$	$2.16^{+0.03}_{-0.04}$	$3.34^{+0.16}_{-0.17}$	$10.30^{+0.07}_{-0.06}$	$2.88^{+0.06}_{-0.06}$	$13.9^{+0.5}_{-0.6}$
13 – 60	$0.60^{+0.02}_{-0.02}$	$2.31^{+0.31}_{-0.32}$	$2.16^{+0.04}_{-0.04}$	$5.00^{+0.43}_{-1.54}$	$7.07^{+0.16}_{-0.15}$	$2.42^{+0.10}_{-0.09}$	$23.2^{+0.9}_{-1.0}$
2 – 13	$0.40^{+0.20}_{-0.04}$	$2.01^{+0.25}_{-0.17}$	$1.89^{+0.04}_{-0.03}$	$3.00^{+0.17}_{-0.13}$	$10.62^{+0.14}_{-0.13}$	$2.97^{+0.09}_{-0.08}$	$13.4^{+0.5}_{-0.5}$
13 – 60	$0.59^{+0.04}_{-0.05}$	$2.16^{+0.35}_{-0.13}$	2.00	$4.71^{+0.55}_{-0.40}$	$6.96^{+0.15}_{-0.21}$	$2.43^{+0.11}_{-0.09}$	$22.9^{+1.0}_{-1.0}$
2 – 13	$0.59^{+0.03}_{-0.02}$	$5.03^{+0.21}_{-2.45}$	1.50	$2.37^{+0.10}_{-0.11}$	$8.81^{+0.13}_{-0.14}$	$3.11^{+0.14}_{-0.09}$	$14.4^{+0.7}_{-0.6}$
13 – 60	$0.58^{+0.04}_{-0.03}$	$2.54^{+1.14}_{-0.49}$	$1.39^{+0.09}_{-0.06}$	$2.00^{+0.63}_{-0.23}$	$5.90^{+0.10}_{-0.21}$	$2.81^{+0.51}_{-0.27}$	$25.1^{+1.3}_{-1.5}$
<i>29/10/1996</i>							
2 – 13	$0.24^{+0.01}_{-0.01}$	$1.87^{+0.13}_{-0.10}$	$1.73^{+0.04}_{-0.03}$	$5.02^{+0.37}_{-1.43}$	$5.74^{+0.08}_{-0.05}$	$2.57^{+0.04}_{-0.04}$	$15.4^{+0.3}_{-0.4}$
13 – 60	$0.25^{+0.01}_{-0.01}$	$1.45^{+0.02}_{-0.01}$	$1.77^{+0.03}_{-0.04}$	$6.38^{+0.34}_{-1.89}$	$5.57^{+0.23}_{-0.45}$	$4.08^{+0.32}_{-0.58}$	$24.4^{+0.5}_{-0.5}$
<i>07/11/1996</i>							
2 – 13	$0.40^{+0.04}_{-0.03}$	$1.97^{+0.22}_{-0.16}$	$2.02^{+0.03}_{-0.15}$	$3.48^{+0.23}_{-0.30}$	$9.80^{+0.07}_{-0.12}$	$2.78^{+0.09}_{-0.07}$	$13.5^{+0.6}_{-0.6}$
13 – 60	$0.41^{+0.02}_{-0.03}$	$1.63^{+0.19}_{-0.14}$	$1.94^{+0.06}_{-0.07}$	$4.23^{+0.65}_{-0.54}$	$6.56^{+0.19}_{-0.23}$	$2.49^{+0.25}_{-0.18}$	$23.0^{+0.8}_{-1.0}$
2 – 13	$0.46^{+0.02}_{-0.03}$	$2.05^{+0.16}_{-0.14}$	$2.19^{+0.04}_{-0.04}$	$3.71^{+0.19}_{-0.18}$	$10.66^{+0.15}_{-0.10}$	$3.00^{+0.08}_{-0.06}$	$13.4^{+0.6}_{-0.5}$
13 – 60	$0.48^{+0.03}_{-0.02}$	$1.83^{+0.17}_{-0.15}$	$2.01^{+0.07}_{-0.04}$	$4.58^{+0.63}_{-0.37}$	$7.17^{+0.11}_{-0.18}$	$2.31^{+0.12}_{-0.07}$	$22.9^{+0.8}_{-0.9}$
2 – 13	$1.57^{+0.05}_{-0.09}$	$2.20^{+0.04}_{-0.07}$	–	–	$17.74^{+0.81}_{-0.74}$	$5.68^{+1.13}_{-1.14}$	$11.0^{+1.0}_{-1.3}$
13 – 60	$1.81^{+0.12}_{-0.06}$	$2.98^{+0.25}_{-0.21}$	–	–	$11.65^{+0.58}_{-0.39}$	$2.44^{+0.35}_{-0.16}$	$17.7^{+1.5}_{-2.0}$
2 – 13	$0.27^{+0.03}_{-0.03}$	$1.76^{+0.23}_{-0.10}$	$1.53^{+0.05}_{-0.07}$	$3.05^{+1.19}_{-0.52}$	$8.60^{+0.21}_{-0.16}$	$2.59^{+0.14}_{-0.12}$	$12.7^{+0.7}_{-0.8}$
13 – 60	$0.49^{+0.07}_{-0.04}$	$2.94^{+2.03}_{-1.06}$	$1.50^{+0.13}_{-0.12}$	$1.99^{+0.51}_{-0.27}$	$6.83^{+0.14}_{-0.87}$	$2.48^{+0.68}_{-0.32}$	$23.3^{+1.0}_{-1.4}$
<i>14/11/1996</i>							
2 – 13	$0.39^{+0.02}_{-0.04}$	$1.82^{+0.24}_{-0.15}$	$1.68^{+0.04}_{-0.04}$	$3.21^{+0.25}_{-0.25}$	$8.55^{+0.08}_{-0.10}$	$2.79^{+0.12}_{-0.07}$	$14.3^{+0.4}_{-0.5}$
13 – 60	$0.39^{+0.02}_{-0.02}$	$1.47^{+0.06}_{-0.04}$	$1.70^{+0.06}_{-0.06}$	$4.82^{+1.04}_{-1.07}$	$5.32^{+0.16}_{-0.03}$	$3.11^{+0.33}_{-0.30}$	$23.5^{+0.7}_{-0.6}$
<i>28/11/1996</i>							
2 – 13	$0.38^{+0.01}_{-0.02}$	$1.82^{+0.11}_{-0.09}$	$1.77^{+0.05}_{-0.03}$	$2.86^{+0.15}_{-0.14}$	$9.68^{+0.10}_{-0.13}$	$2.79^{+0.08}_{-0.06}$	$13.5^{+0.5}_{-0.4}$
13 – 60	$0.35^{+0.05}_{-0.05}$	$1.41^{+0.04}_{-0.03}$	$1.46^{+0.03}_{-0.05}$	$2.79^{+0.27}_{-0.17}$	$6.73^{+0.12}_{-0.08}$	$3.39^{+0.40}_{-0.31}$	$22.2^{+0.6}_{-0.6}$
<i>04/12/1996</i>							
2 – 13	$0.20^{+0.01}_{-0.01}$	$1.91^{+0.26}_{-0.22}$	$1.43^{+0.03}_{-0.02}$	$1.90^{+0.07}_{-0.05}$	$5.13^{+0.10}_{-0.10}$	$2.63^{+0.11}_{-0.12}$	$18.0^{+0.6}_{-0.6}$
13 – 60	$0.20^{+0.01}_{-0.01}$	$1.43^{+0.06}_{-0.03}$	$1.01^{+0.08}_{-0.04}$	$3.18^{+1.02}_{-0.99}$	$3.17^{+0.09}_{-0.02}$	$2.59^{+0.15}_{-0.14}$	$23.6^{+0.8}_{-0.8}$
<i>11/12/1996</i>							
2 – 13	$0.19^{+0.02}_{-0.01}$	$1.77^{+0.25}_{-0.12}$	$1.34^{+0.02}_{-0.03}$	$2.55^{+0.22}_{-0.37}$	$4.86^{+0.17}_{-0.10}$	$2.08^{+0.07}_{-0.04}$	$16.3^{+0.7}_{-0.8}$
13 – 60	$0.20^{+0.01}_{-0.01}$	$1.49^{+0.09}_{-0.08}$	$1.01^{+0.05}_{-0.04}$	$3.59^{+0.49}_{-0.37}$	$3.07^{+0.21}_{-0.08}$	$2.01^{+0.14}_{-0.18}$	$21.2^{+0.9}_{-0.9}$
<i>19/12/1996</i>							
2 – 13	$0.26^{+0.01}_{-0.01}$	$3.87^{+0.60}_{-0.35}$	$1.15^{+0.03}_{-0.03}$	$2.22^{+0.21}_{-0.16}$	$5.96^{+0.08}_{-0.13}$	$2.20^{+0.04}_{-0.04}$	$15.6^{+0.6}_{-0.7}$
13 – 60	$0.26^{+0.01}_{-0.01}$	$2.59^{+0.14}_{-0.27}$	$1.10^{+0.02}_{-0.02}$	$3.84^{+0.08}_{-0.82}$	$3.66^{+0.35}_{-0.10}$	$2.04^{+0.06}_{-0.06}$	$21.5^{+0.8}_{-0.9}$
<i>24/12/1996</i>							
2 – 13	$0.31^{+0.04}_{-0.02}$	$2.71^{+0.81}_{-0.50}$	$1.47^{+0.03}_{-0.05}$	$2.22^{+0.18}_{-0.19}$	$8.10^{+0.13}_{-0.11}$	$2.60^{+0.14}_{-0.08}$	$14.8^{+0.5}_{-0.4}$
13 – 60	$0.38^{+0.01}_{-0.01}$	$4.15^{+0.73}_{-0.97}$	$1.34^{+0.03}_{-0.02}$	$3.46^{+0.37}_{-0.35}$	$4.81^{+0.14}_{-0.05}$	$2.18^{+0.08}_{-0.07}$	$21.0^{+0.9}_{-0.9}$
<i>31/12/1996</i>							
2 – 13	$0.22^{+0.02}_{-0.01}$	$2.96^{+0.49}_{-0.47}$	$1.32^{+0.02}_{-0.02}$	$1.73^{+0.05}_{-0.04}$	$5.48^{+0.06}_{-0.11}$	$2.74^{+0.13}_{-0.15}$	$17.9^{+0.6}_{-0.5}$
13 – 60	$0.22^{+0.01}_{-0.01}$	$1.80^{+0.24}_{-0.20}$	$1.07^{+0.04}_{-0.04}$	$5.47^{+1.00}_{-1.98}$	$3.20^{+0.12}_{-0.06}$	$2.17^{+0.09}_{-0.06}$	$21.0^{+0.6}_{-0.8}$
<i>07/01/1997</i>							
2 – 13	$0.22^{+0.01}_{-0.01}$	$2.10^{+0.35}_{-0.29}$	$1.45^{+0.03}_{-0.01}$	$1.73^{+0.05}_{-0.03}$	$5.57^{+0.05}_{-0.09}$	$2.73^{+0.12}_{-0.12}$	$17.4^{+0.5}_{-0.5}$
13 – 60	$0.21^{+0.03}_{-0.01}$	$1.46^{+0.18}_{-0.10}$	$1.07^{+0.06}_{-0.03}$	$2.71^{+1.01}_{-0.62}$	$3.69^{+0.24}_{-0.11}$	$2.24^{+0.19}_{-0.15}$	$19.5^{+0.8}_{-0.8}$
<i>14/01/1997</i>							
2 – 13	$0.26^{+0.02}_{-0.01}$	$2.47^{+0.67}_{-0.54}$	$1.48^{+0.04}_{-0.04}$	$1.70^{+0.07}_{-0.04}$	$5.50^{+0.12}_{-0.16}$	$2.84^{+0.17}_{-0.19}$	$17.8^{+0.6}_{-0.5}$
13 – 60	$0.28^{+0.01}_{-0.01}$	$2.87^{+0.58}_{-0.43}$	$0.94^{+0.04}_{-0.04}$	$1.50^{+0.10}_{-0.07}$	$3.77^{+0.15}_{-0.13}$	$2.89^{+0.41}_{-0.29}$	$19.7^{+0.8}_{-0.6}$

Table 4: The characteristics of the power density spectrum. (continued) Parameter errors and upper limits correspond to the  $1\sigma$  and  $2\sigma$  confidence levels respectively.

Energy (keV)	$f_1^{br}$ (Hz)	$\alpha_1$	$f_2^{br}$ (Hz)	$\alpha_2$	$f_3^{br}$ (Hz)	$\alpha_3$	$rms_{BLN}$ (%)
<i>23/01/1997</i>							
2 – 13	$0.23^{+0.01}_{-0.01}$	$3.20^{+0.54}_{-0.40}$	$1.37^{+0.02}_{-0.04}$	$1.67^{+0.04}_{-0.03}$	$5.38^{+0.09}_{-0.08}$	$2.81^{+0.12}_{-0.12}$	$18.2^{+0.6}_{-0.4}$
13 – 60	$0.22^{+0.02}_{-0.01}$	$1.91^{+0.31}_{-0.26}$	$0.98^{+0.04}_{-0.02}$	$1.39^{+0.05}_{-0.04}$	$3.80^{+0.09}_{-0.11}$	$3.40^{+0.40}_{-0.36}$	$19.1^{+0.8}_{-0.7}$
<i>29/01/1997</i>							
2 – 13	$0.30^{+0.01}_{-0.01}$	$1.74^{+0.29}_{-0.37}$	1.40	$1.68^{+0.06}_{-0.04}$	$7.40^{+0.09}_{-0.11}$	$3.14^{+0.25}_{-0.22}$	$15.3^{+0.7}_{-0.6}$
13 – 60	$0.34^{+0.03}_{-0.02}$	$1.94^{+0.28}_{-0.33}$	$1.23^{+0.04}_{-0.03}$	$1.54^{+0.10}_{-0.06}$	$5.21^{+0.16}_{-0.22}$	$3.40^{+0.77}_{-0.74}$	$18.9^{+1.0}_{-0.9}$
<i>01/02/1997</i>							
2 – 13	$0.25^{+0.02}_{-0.02}$	$1.50^{+0.18}_{-0.14}$	$1.31^{+0.06}_{-0.04}$	$1.71^{+0.12}_{-0.07}$	$6.95^{+0.10}_{-0.10}$	$2.86^{+0.17}_{-0.17}$	$15.5^{+0.6}_{-0.5}$
13 – 60	$0.27^{+0.02}_{-0.02}$	$1.26^{+0.03}_{-0.04}$	$1.18^{+0.03}_{-0.02}$	$4.18^{+1.00}_{-0.80}$	$4.45^{+0.10}_{-0.10}$	$3.73^{+0.29}_{-0.31}$	$19.2^{+0.8}_{-0.8}$
<i>09/02/1997</i>							
2 – 13	$0.15^{+0.01}_{-0.01}$	$1.85^{+0.26}_{-0.20}$	$1.55^{+0.07}_{-0.06}$	$1.61^{+0.03}_{-0.03}$	$4.50^{+0.04}_{-0.04}$	$2.71^{+0.06}_{-0.08}$	$19.6^{+0.5}_{-0.4}$
13 – 60	$0.17^{+0.01}_{-0.01}$	$1.32^{+0.07}_{-0.05}$	$1.43^{+0.13}_{-0.06}$	$2.31^{+0.23}_{-0.27}$	$3.37^{+0.19}_{-0.20}$	$2.23^{+0.18}_{-0.19}$	$18.0^{+0.8}_{-0.7}$
<i>22/02/1997</i>							
2 – 13	$0.20^{+0.03}_{-0.03}$	$1.17^{+0.29}_{-0.07}$	$1.62^{+0.09}_{-0.09}$	$1.76^{+0.46}_{-0.22}$	$5.74^{+0.08}_{-0.08}$	$3.05^{+0.21}_{-0.19}$	$18.0^{+0.6}_{-0.7}$
13 – 60	$0.25^{+0.04}_{-0.05}$	$1.26^{+0.05}_{-0.04}$	$1.03^{+0.05}_{-0.06}$	$5.05^{+0.95}_{-1.05}$	$3.84^{+0.20}_{-0.12}$	$2.94^{+0.37}_{-0.15}$	$18.0^{+0.7}_{-0.8}$
<i>05/03/1997</i>							
2 – 13	$0.23^{+0.01}_{-0.02}$	$1.98^{+0.58}_{-0.41}$	$1.65^{+0.06}_{-0.11}$	$1.69^{+0.10}_{-0.08}$	$6.23^{+0.10}_{-0.17}$	$3.02^{+0.24}_{-0.25}$	$17.1^{+0.5}_{-0.4}$
13 – 60	$0.25^{+0.02}_{-0.02}$	$1.24^{+0.81}_{-0.05}$	$0.95^{+0.08}_{-0.07}$	$2.14^{+1.50}_{-0.75}$	$4.75^{+0.11}_{-0.20}$	$3.58^{+1.16}_{-0.63}$	$18.2^{+0.8}_{-0.7}$
<i>10/03/1997</i>							
2 – 13	$0.17^{+0.02}_{-0.04}$	$2.06^{+0.50}_{-0.42}$	1.60	$1.63^{+0.04}_{-0.04}$	$4.35^{+0.07}_{-0.07}$	$2.65^{+0.10}_{-0.09}$	$20.2^{+0.7}_{-0.5}$
13 – 60	$0.16^{+0.02}_{-0.02}$	$1.26^{+0.05}_{-0.04}$	–	–	$2.47^{+0.05}_{-0.05}$	$2.15^{+0.13}_{-0.09}$	$18.5^{+0.8}_{-0.6}$
<i>17/03/1997</i>							
2 – 13	$0.24^{+0.01}_{-0.01}$	$1.90^{+0.33}_{-0.36}$	$1.66^{+0.06}_{-0.07}$	$1.60^{+0.04}_{-0.03}$	$6.35^{+0.10}_{-0.10}$	$3.35^{+0.25}_{-0.51}$	$17.3^{+0.6}_{-0.7}$
13 – 60	$0.26^{+0.01}_{-0.01}$	$1.51^{+0.41}_{-0.06}$	$0.98^{+0.07}_{-0.06}$	$1.39^{+1.80}_{-0.08}$	$4.32^{+0.06}_{-0.12}$	$3.91^{+0.50}_{-0.64}$	$18.1^{+0.8}_{-0.9}$
<i>26/03/1997</i>							
2 – 13	$0.34^{+0.03}_{-0.02}$	$2.51^{+0.56}_{-0.62}$	$1.74^{+0.07}_{-0.09}$	$1.68^{+0.06}_{-0.05}$	$7.28^{+0.11}_{-0.20}$	$3.91^{+0.53}_{-0.47}$	$16.4^{+0.6}_{-0.6}$
13 – 60	$0.37^{+0.03}_{-0.02}$	$2.12^{+0.73}_{-0.58}$	$1.18^{+0.16}_{-0.10}$	$1.27^{+0.08}_{-0.09}$	$4.79^{+0.09}_{-0.21}$	$4.00^{+1.02}_{-0.97}$	$18.0^{+0.9}_{-0.9}$
<i>27/03/1997</i>							
2 – 13	$0.34^{+0.02}_{-0.02}$	$3.78^{+1.16}_{-0.86}$	1.80	$2.34^{+0.39}_{-0.34}$	$7.25^{+0.15}_{-0.26}$	$2.66^{+0.27}_{-0.27}$	$15.9^{+0.6}_{-0.6}$
13 – 60	$0.33^{+0.03}_{-0.02}$	$1.91^{+0.71}_{-0.41}$	$1.34^{+0.08}_{-0.08}$	$4.20^{+0.51}_{-1.78}$	$4.87^{+0.23}_{-0.18}$	$2.38^{+0.29}_{-0.18}$	$18.0^{+0.9}_{-0.8}$
<i>02/04/1997*</i>							
2 – 13	$1.01^{+0.03}_{-0.03}$	$1.67^{+0.13}_{-0.06}$	–	–	$10.35^{+0.28}_{-0.23}$	$3.52^{+0.38}_{-0.38}$	$11.4^{+0.5}_{-0.5}$
13 – 60	$0.81^{+0.04}_{-0.01}$	$1.47^{+0.05}_{-0.03}$	–	–	$6.78^{+0.56}_{-0.80}$	$3.55^{+0.60}_{-0.43}$	$16.7^{+0.8}_{-0.9}$
<i>10/04/1997*</i>							
2 – 13	$0.95^{+0.08}_{-0.05}$	$1.66^{+0.13}_{-0.10}$	–	–	$10.98^{+0.43}_{-0.43}$	$4.73^{+0.56}_{-1.22}$	$10.9^{+0.6}_{-0.7}$
13 – 60	$0.67^{+0.04}_{-0.04}$	$1.41^{+0.08}_{-0.07}$	–	–	$5.55^{+0.18}_{-0.18}$	$3.85^{+0.75}_{-0.50}$	$18.4^{+0.9}_{-1.0}$
<i>19/04/1997</i>							
2 – 13	$0.17^{+0.02}_{-0.01}$	$2.21^{+0.54}_{-0.44}$	$1.31^{+0.12}_{-0.05}$	$1.58^{+0.06}_{-0.04}$	$5.10^{+0.11}_{-0.10}$	$2.82^{+0.18}_{-0.17}$	$17.8^{+0.6}_{-0.7}$
13 – 60	$0.19^{+0.01}_{-0.03}$	$1.63^{+0.27}_{-0.25}$	$1.28^{+0.02}_{-0.20}$	$3.39^{+0.59}_{-0.94}$	$4.50^{+0.20}_{-0.14}$	$2.00^{+0.05}_{-0.02}$	$17.2^{+0.8}_{-0.9}$
<i>23/04/1997</i>							
2 – 13	$0.22^{+0.02}_{-0.01}$	$2.96^{+0.79}_{-0.64}$	$1.42^{+0.05}_{-0.05}$	$1.77^{+0.13}_{-0.07}$	$4.97^{+0.16}_{-0.19}$	$2.46^{+0.18}_{-0.19}$	$18.0^{+0.5}_{-0.6}$
13 – 60	$0.20^{+0.01}_{-0.02}$	$1.62^{+0.28}_{-0.06}$	$0.87^{+0.03}_{-0.03}$	$1.47^{+0.26}_{-0.07}$	$4.00^{+0.15}_{-0.17}$	$3.14^{+0.65}_{-0.48}$	$18.3^{+0.7}_{-0.7}$
<i>25/04/1997</i>							
2 – 13	$0.34^{+0.01}_{-0.01}$	$1.56^{+0.11}_{-0.08}$	$1.63^{+0.03}_{-0.02}$	$3.18^{+0.26}_{-0.24}$	$8.92^{+0.07}_{-0.07}$	$2.81^{+0.12}_{-0.11}$	$13.5^{+0.5}_{-0.5}$
13 – 60	$0.34^{+0.01}_{-0.01}$	$1.37^{+0.06}_{-0.04}$	$1.48^{+0.06}_{-0.03}$	$4.23^{+0.54}_{-0.58}$	$5.80^{+0.16}_{-0.19}$	$3.39^{+0.41}_{-0.42}$	$18.8^{+0.8}_{-0.7}$

\* – for these observations the additional power law noise component was included to the fit to describe the low frequency part of the power density spectrum.

Table 5: The characteristics of the power density spectrum not included to the Tables 3, 4.

$f_{QPO}$ (Hz)	FWHM (Hz)	$rms_1^{QPO}$ (%)	$rms_{1/2}^{QPO}$ (%)	$rms_2^{QPO}$ (%)	$rms_3^{QPO}$ (%)	$\chi^2(d.o.f)$
<i>23/10/1996</i>						
$5.02^{+0.01}_{-0.02}$	$0.71^{+0.03}_{-0.04}$	$5.9^{+0.4}_{-0.5}$	< 2.5	< 1.5	< 1.0	381.0(205)
$5.14^{+0.07}_{-0.03}$	$0.66^{+0.09}_{-0.07}$	$7.0^{+0.6}_{-0.5}$	$3.7^{+0.8}_{-0.7}$	< 2.2	< 1.7	256.0(144)
$5.07^{+0.01}_{-0.01}$	$0.66^{+0.04}_{-0.03}$	$5.4^{+0.5}_{-0.5}$	$1.9^{+0.6}_{-0.6}$	< 2.0	< 1.2	371.(205)
$5.15^{+0.10}_{-0.10}$	$0.83^{+0.10}_{-0.10}$	$7.0^{+0.6}_{-0.6}$	$3.5^{+0.7}_{-0.8}$	$2.3^{+0.8}_{-0.7}$	< 1.8	268.5(144)
$5.12^{+0.02}_{-0.01}$	$0.77^{+0.05}_{-0.04}$	$5.4^{+0.5}_{-0.5}$	$2.3^{+0.5}_{-0.5}$	< 2.1	< 1.0	322.7(205)
$5.20^{+0.05}_{-0.10}$	$0.79^{+0.10}_{-0.10}$	$6.8^{+0.5}_{-0.7}$	$3.8^{+0.9}_{-0.7}$	< 2.5	< 2.0	234.5(144)
$4.45^{+0.01}_{-0.01}$	$0.70^{+0.04}_{-0.04}$	$7.2^{+0.6}_{-0.5}$	$2.9^{+0.4}_{-0.4}$	< 2.0	< 1.3	383.1(205)
$4.51^{+0.03}_{-0.02}$	$0.64^{+0.07}_{-0.06}$	$8.6^{+0.5}_{-0.5}$	$4.0^{+0.9}_{-0.6}$	< 2.0	< 2.5	237.8(144)
<i>29/10/1996</i>						
$3.22^{+0.01}_{-0.01}$	$0.65^{+0.01}_{-0.02}$	$12.2^{+0.2}_{-0.3}$	< 0.5	$3.5^{+0.3}_{-0.3}$	$0.8^{+0.4}_{-0.4}$	251.7(205)
$3.23^{+0.01}_{-0.01}$	$0.69^{+0.01}_{-0.02}$	$16.2^{+0.3}_{-0.4}$	< 1.2	$2.7^{+0.7}_{-0.6}$	$2.4^{+0.7}_{-0.8}$	207.1(144)
<i>07/11/1996</i>						
$4.81^{+0.01}_{-0.01}$	$0.57^{+0.02}_{-0.03}$	$6.4^{+0.5}_{-0.6}$	$1.5^{+0.5}_{-0.6}$	< 2.3	< 1.9	380.8(205)
$4.88^{+0.02}_{-0.05}$	$0.51^{+0.05}_{-0.05}$	$7.5^{+0.6}_{-0.5}$	$2.2^{+0.6}_{-0.5}$	< 3.0	< 1.3	238.3(144)
$5.08^{+0.01}_{-0.01}$	$0.68^{+0.02}_{-0.02}$	$5.9^{+0.5}_{-0.5}$	$1.5^{+0.5}_{-0.5}$	< 2.0	< 1.3	430.9(205)
$5.15^{+0.05}_{-0.08}$	$0.71^{+0.06}_{-0.06}$	$7.4^{+0.6}_{-0.6}$	$3.5^{+0.8}_{-0.8}$	$2.5^{+0.4}_{-0.5}$	< 1.6	321.3(144)
$7.83^{+0.04}_{-0.04}$	$0.80^{+0.10}_{-0.08}$	$2.6^{+0.5}_{-0.6}$	—	—	—	272.5(178)
$7.83^{+0.04}_{-0.04}$	$0.98^{+0.14}_{-0.14}$	$7.4^{+0.8}_{-0.9}$	—	—	—	137.7(93)
$4.20^{+0.03}_{-0.03}$	$1.22^{+0.10}_{-0.10}$	$8.7^{+0.6}_{-0.6}$	$3.5^{+0.8}_{-0.9}$	< 2.3	< 1.8	290.7(205)
$4.25^{+0.05}_{-0.05}$	$1.20^{+0.20}_{-0.19}$	$11.1^{+0.7}_{-0.7}$	$4.8^{+0.8}_{-0.7}$	—	—	107.6(88)
<i>14/11/1996</i>						
$4.25^{+0.02}_{-0.02}$	$0.68^{+0.03}_{-0.03}$	$8.0^{+0.3}_{-0.3}$	$2.5^{+0.5}_{-0.5}$	< 1.0	< 1.0	304.9(205)
$4.28^{+0.01}_{-0.03}$	$0.63^{+0.06}_{-0.05}$	$8.6^{+0.5}_{-0.5}$	$3.1^{+0.8}_{-0.9}$	$2.2^{+0.8}_{-0.8}$	< 2.0	240.2(144)
<i>28/11/1996</i>						
$4.63^{+0.03}_{-0.01}$	$0.94^{+0.02}_{-0.03}$	$7.9^{+0.2}_{-0.2}$	$2.4^{+0.3}_{-0.4}$	< 1.5	< 1.0	356.1(205)
$4.65^{+0.02}_{-0.02}$	$1.03^{+0.05}_{-0.06}$	$9.4^{+0.3}_{-0.3}$	$3.2^{+0.7}_{-0.7}$	< 1.6	< 2.0	224.7(144)
<i>04/12/1996</i>						
$2.81^{+0.01}_{-0.01}$	$0.41^{+0.01}_{-0.01}$	$11.1^{+0.4}_{-0.4}$	$2.2^{+0.3}_{-0.4}$	$5.0^{+0.2}_{-0.3}$	$1.5^{+0.3}_{-0.3}$	418.2(208)
$2.81^{+0.01}_{-0.01}$	$0.42^{+0.02}_{-0.02}$	$13.5^{+0.4}_{-0.5}$	$2.3^{+0.7}_{-0.7}$	$3.4^{+0.5}_{-0.4}$	< 1.6	164.1(144)
<i>11/12/1996</i>						
$2.77^{+0.01}_{-0.01}$	$0.81^{+0.02}_{-0.02}$	$13.0^{+0.1}_{-0.3}$	< 2.2	$6.3^{+0.05}_{-0.05}$	$2.3^{+0.4}_{-0.3}$	290.6(205)
$2.78^{+0.01}_{-0.01}$	$0.80^{+0.04}_{-0.03}$	$14.9^{+0.5}_{-0.3}$	$2.6^{+0.5}_{-0.4}$	$4.00^{+0.5}_{-0.4}$	< 1.4	176.6(144)
<i>19/12/1996</i>						
$3.11^{+0.01}_{-0.01}$	$0.76^{+0.03}_{-0.02}$	$12.1^{+0.3}_{-0.2}$	$3.7^{+0.5}_{-0.5}$	$5.5^{+0.2}_{-0.3}$	$2.1^{+0.5}_{-0.4}$	235.5(205)
$3.12^{+0.01}_{-0.01}$	$0.73^{+0.03}_{-0.03}$	$13.3^{+0.5}_{-0.3}$	$3.2^{+0.9}_{-1.0}$	$3.1^{+0.5}_{-0.5}$	< 1.1	147.9(144)
<i>24/12/1996</i>						
$3.90^{+0.01}_{-0.01}$	$0.79^{+0.03}_{-0.03}$	$10.2^{+0.3}_{-0.3}$	$2.5^{+0.5}_{-0.5}$	$2.7^{+0.4}_{-0.4}$	$1.1^{+0.4}_{-0.4}$	362.3(205)
$3.91^{+0.02}_{-0.01}$	$0.74^{+0.05}_{-0.04}$	$10.3^{+0.4}_{-0.4}$	$2.6^{+0.8}_{-0.8}$	< 1.0	< 1.0	209.5(144)
<i>31/12/1996</i>						
$2.80^{+0.01}_{-0.01}$	$0.61^{+0.02}_{-0.03}$	$11.8^{+0.2}_{-0.4}$	$2.9^{+0.6}_{-0.5}$	$6.2^{+0.9}_{-1.0}$	$2.1^{+0.4}_{-0.4}$	229.4(205)
$2.81^{+0.01}_{-0.01}$	$0.50^{+0.03}_{-0.02}$	$11.9^{+0.4}_{-0.4}$	$2.7^{+0.8}_{-0.8}$	$2.9^{+0.5}_{-0.5}$	< 1.0	132.8(144)
<i>07/01/1997</i>						
$2.91^{+0.01}_{-0.01}$	$0.67^{+0.02}_{-0.02}$	$12.1^{+0.6}_{-0.3}$	$2.3^{+0.6}_{-0.6}$	$5.9^{+0.2}_{-0.2}$	$2.1^{+0.3}_{-0.3}$	298.0(205)
$2.91^{+0.01}_{-0.01}$	$0.57^{+0.03}_{-0.02}$	$12.0^{+0.4}_{-0.4}$	$2.7^{+0.3}_{-0.3}$	$3.1^{+0.5}_{-0.5}$	< 1.0	170.6(144)
<i>14/01/1997</i>						
$2.92^{+0.01}_{-0.01}$	$0.63^{+0.03}_{-0.04}$	$11.6^{+0.3}_{-0.4}$	$2.1^{+0.8}_{-0.6}$	$5.5^{+0.3}_{-0.3}$	$1.9^{+0.3}_{-0.3}$	220.5(205)
$2.92^{+0.01}_{-0.01}$	$0.54^{+0.04}_{-0.03}$	$11.1^{+0.4}_{-0.4}$	$2.1^{+0.6}_{-0.6}$	$2.5^{+0.3}_{-0.3}$	< 1.0	163.7(144)
<i>23/01/1997</i>						
$2.80^{+0.01}_{-0.01}$	$0.58^{+0.01}_{-0.02}$	$12.0^{+0.3}_{-0.3}$	$2.2^{+0.6}_{-0.5}$	$4.5^{+0.4}_{-0.4}$	< 2.2	316.2(205)
$2.80^{+0.01}_{-0.01}$	$0.48^{+0.03}_{-0.02}$	$11.4^{+0.3}_{-0.3}$	$2.3^{+0.5}_{-0.5}$	$3.5^{+0.5}_{-0.6}$	< 1.0	157.2(144)

Table 6: The characteristics of the power density spectrum not included to the Tables 3, 4. (continued)

$f_{QPO}$ (Hz)	FWHM (Hz)	$rms_1^{QPO}$ (%)	$rms_{1/2}^{QPO}$ (%)	$rms_2^{QPO}$ (%)	$rms_3^{QPO}$ (%)	$\chi^2(d.o.f)$
<i>29/01/1997</i>						
$3.64^{+0.02}_{-0.01}$	$0.99^{+0.03}_{-0.02}$	$11.4^{+0.2}_{-0.3}$	$3.2^{+0.4}_{-0.4}$	$3.6^{+0.8}_{-0.9}$	$1.6^{+0.5}_{-0.6}$	296.0(202)
$3.67^{+0.01}_{-0.02}$	$0.90^{+0.04}_{-0.05}$	$11.0^{+0.3}_{-0.3}$	$1.9^{+0.6}_{-0.6}$	$1.8^{+0.6}_{-0.6}$	< 1.5	200.7(145)
<i>01/02/1997</i>						
$3.56^{+0.01}_{-0.01}$	$0.96^{+0.03}_{-0.03}$	$11.4^{+0.2}_{-0.2}$	$3.7^{+0.4}_{-0.4}$	$3.8^{+0.4}_{-0.4}$	$1.3^{+0.4}_{-0.3}$	342.8(205)
$3.55^{+0.01}_{-0.01}$	$0.72^{+0.04}_{-0.05}$	$10.0^{+0.3}_{-0.3}$	$2.9^{+0.6}_{-0.5}$	$3.0^{+0.6}_{-0.6}$	< 2.0	195.8(144)
<i>09/02/1997</i>						
$2.26^{+0.01}_{-0.01}$	$0.43^{+0.01}_{-0.01}$	$12.4^{+0.3}_{-0.3}$	$2.6^{+0.4}_{-0.3}$	$5.4^{+0.2}_{-0.2}$	$2.0^{+0.6}_{-0.5}$	251.5(205)
$2.26^{+0.01}_{-0.01}$	$0.45^{+0.02}_{-0.02}$	$12.4^{+0.3}_{-0.3}$	$1.6^{+0.7}_{-0.6}$	$4.0^{+0.4}_{-0.4}$	$1.5^{+0.5}_{-0.5}$	158.5(144)
<i>22/02/1997</i>						
$2.98^{+0.01}_{-0.01}$	$0.61^{+0.02}_{-0.02}$	$11.3^{+0.3}_{-0.3}$	$3.2^{+0.5}_{-0.4}$	$4.0^{+0.6}_{-0.5}$	< 0.8	232.4(205)
$2.98^{+0.01}_{-0.01}$	$0.51^{+0.03}_{-0.03}$	$10.3^{+0.3}_{-0.3}$	$3.3^{+0.6}_{-0.6}$	$2.9^{+0.6}_{-0.6}$	< 1.3	175.4(144)
<i>05/03/1997</i>						
$3.24^{+0.01}_{-0.01}$	$0.64^{+0.04}_{-0.03}$	$11.1^{+0.4}_{-0.4}$	$2.9^{+0.8}_{-0.7}$	$3.8^{+0.7}_{-0.7}$	< 1.1	270.1(205)
$3.25^{+0.01}_{-0.01}$	$0.61^{+0.05}_{-0.04}$	$11.0^{+0.4}_{-0.3}$	$3.4^{+0.8}_{-0.8}$	$1.8^{+0.6}_{-0.6}$	< 2.2	123.1(144)
<i>10/03/1997</i>						
$2.21^{+0.01}_{-0.01}$	$0.35^{+0.02}_{-0.02}$	$12.2^{+0.4}_{-0.4}$	$2.4^{+0.5}_{-0.5}$	$5.5^{+0.4}_{-0.4}$	< 1.0	257.4(205)
$2.21^{+0.01}_{-0.01}$	$0.33^{+0.01}_{-0.02}$	$11.1^{+0.4}_{-0.4}$	$2.4^{+0.5}_{-0.5}$	$3.7^{+0.4}_{-0.3}$	< 1.2	139.7(144)
<i>17/03/1997</i>						
$3.21^{+0.01}_{-0.01}$	$0.64^{+0.03}_{-0.03}$	$11.3^{+0.4}_{-0.4}$	$2.8^{+0.5}_{-0.5}$	$4.0^{+0.4}_{-0.4}$	< 1.5	256.3(205)
$3.21^{+0.01}_{-0.01}$	$0.58^{+0.03}_{-0.03}$	$10.8^{+0.4}_{-0.3}$	$2.7^{+0.4}_{-0.5}$	$3.3^{+0.5}_{-0.5}$	< 1.4	140.3(144)
<i>26/03/1997</i>						
$3.52^{+0.01}_{-0.01}$	$0.71^{+0.05}_{-0.03}$	$10.6^{+0.4}_{-0.5}$	$1.7^{+0.8}_{-0.7}$	$3.1^{+0.6}_{-0.6}$	$1.8^{+0.6}_{-0.6}$	214.0(205)
$3.52^{+0.01}_{-0.01}$	$0.70^{+0.06}_{-0.07}$	$10.3^{+0.5}_{-0.5}$	$2.3^{+1.1}_{-0.9}$	$2.3^{+0.5}_{-0.6}$	< 1.5	145.8(144)
<i>27/03/1997</i>						
$3.65^{+0.01}_{-0.01}$	$0.84^{+0.05}_{-0.04}$	$10.9^{+0.5}_{-0.5}$	< 1.5	$3.3^{+0.8}_{-0.8}$	< 1.5	206.0(205)
$3.64^{+0.01}_{-0.01}$	$0.77^{+0.07}_{-0.07}$	$10.7^{+0.3}_{-0.5}$	$3.0^{+0.6}_{-0.7}$	$2.5^{+0.5}_{-0.6}$	< 1.3	129.2(144)
<i>02/04/1997</i>						
$4.90^{+0.01}_{-0.03}$	$1.47^{+0.06}_{-0.05}$	$9.2^{+0.3}_{-0.3}$	$3.4^{+0.4}_{-0.4}$	$2.1^{+0.7}_{-0.7}$	$1.3^{+0.6}_{-0.6}$	311.2(206)
$4.86^{+0.03}_{-0.02}$	$1.60^{+0.12}_{-0.05}$	$10.4^{+0.5}_{-0.5}$	$2.4^{+0.8}_{-0.8}$	< 2.1	< 1.5	168.8(144)
<i>10/04/1997*</i>						
$4.44^{+0.01}_{-0.01}$	$1.29^{+0.05}_{-0.05}$	$10.6^{+0.4}_{-0.4}$	$4.1^{+0.4}_{-0.4}$	$4.1^{+0.6}_{-0.6}$	< 2.4	283.9(206)
$4.45^{+0.03}_{-0.03}$	$0.82^{+0.12}_{-0.10}$	$8.3^{+0.5}_{-0.6}$	< 3.0	$2.9^{+0.9}_{-0.9}$	< 3.0	179.7(148)
<i>19/04/1997</i>						
$2.53^{+0.01}_{-0.01}$	$0.61^{+0.03}_{-0.03}$	$12.8^{+0.4}_{-0.4}$	$2.2^{+0.8}_{-0.7}$	$5.6^{+0.6}_{-0.5}$	< 0.7	209.8(205)
$2.55^{+0.01}_{-0.02}$	$0.77^{+0.04}_{-0.04}$	$13.4^{+0.4}_{-0.3}$	$1.2^{+0.6}_{-0.5}$	$3.4^{+0.6}_{-0.7}$	< 1.0	176.5(144)
<i>23/04/1997</i>						
$2.72^{+0.01}_{-0.01}$	$0.59^{+0.03}_{-0.03}$	$12.3^{+0.4}_{-0.4}$	$1.7^{+0.8}_{-0.8}$	$5.4^{+0.6}_{-0.6}$	< 1.3	233.0(205)
$2.71^{+0.01}_{-0.01}$	$0.58^{+0.03}_{-0.03}$	$12.5^{+0.5}_{-0.4}$	$2.8^{+0.7}_{-0.7}$	$3.7^{+0.3}_{-0.4}$	< 1.7	120.5(144)
<i>25/04/1997</i>						
$4.27^{+0.01}_{-0.01}$	$1.14^{+0.03}_{-0.03}$	$9.9^{+0.2}_{-0.2}$	$3.1^{+0.4}_{-0.4}$	$5.9^{+0.5}_{-0.4}$	$1.3^{+0.4}_{-0.3}$	458.0(205)
$4.28^{+0.02}_{-0.01}$	$1.05^{+0.06}_{-0.06}$	$9.9^{+0.3}_{-0.2}$	$2.8^{+0.6}_{-0.6}$	$2.5^{+0.5}_{-0.4}$	$1.7^{+0.8}_{-0.9}$	232.5(144)

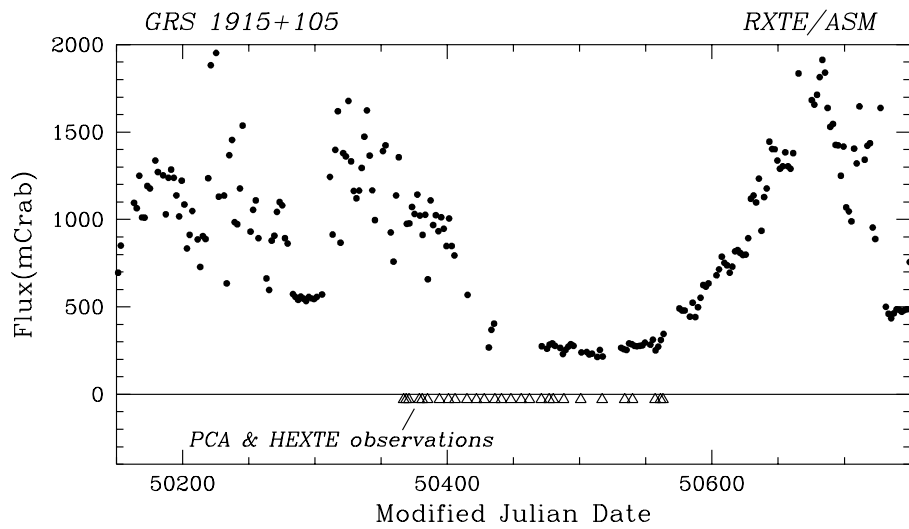


Figure 1: The *RXTE*/*ASM* light curve of GRS 1915+105 in the 2–12 keV energy band. The dates of the pointed PCA and HEXTE observations are marked with triangles. These particular observations were chosen in order to cover the period of extended low luminosity state (hereafter LLS) of the source and the transition from and to higher luminosity states (hereafter HLS).

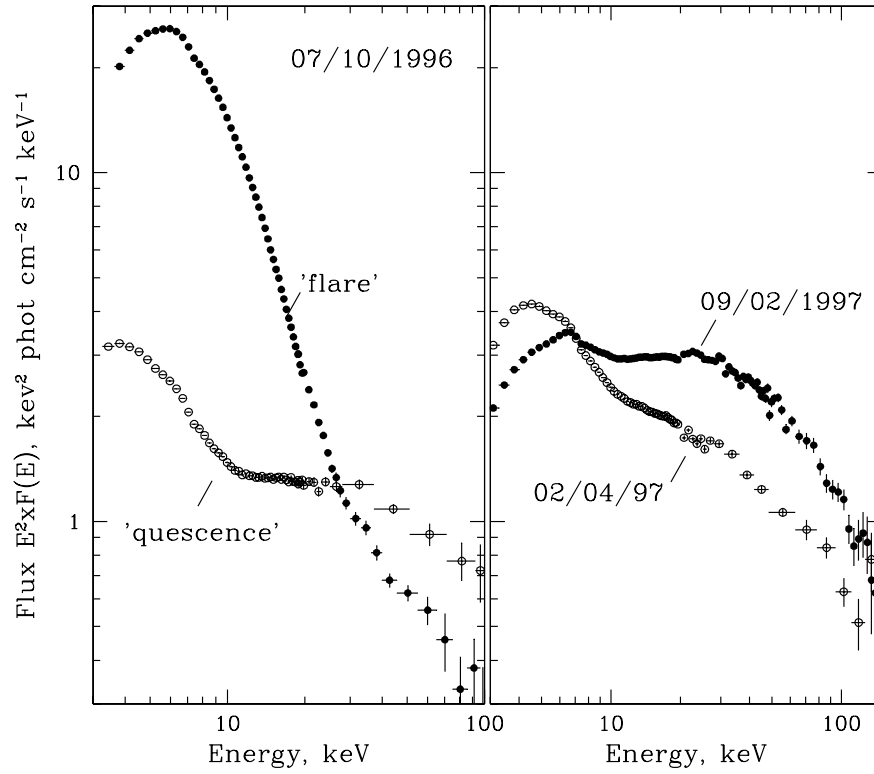


Figure 2: Typical broad-band energy spectra of GRS 1915+105 in the high luminosity 'flaring' (*left panel*) and low luminosity (*right panel*) states (PCA and HEXTE data). Open and solid circles in the *left panel* represent the data for the high ('outburst') and low ('quiescence') levels of source luminosity respectively.

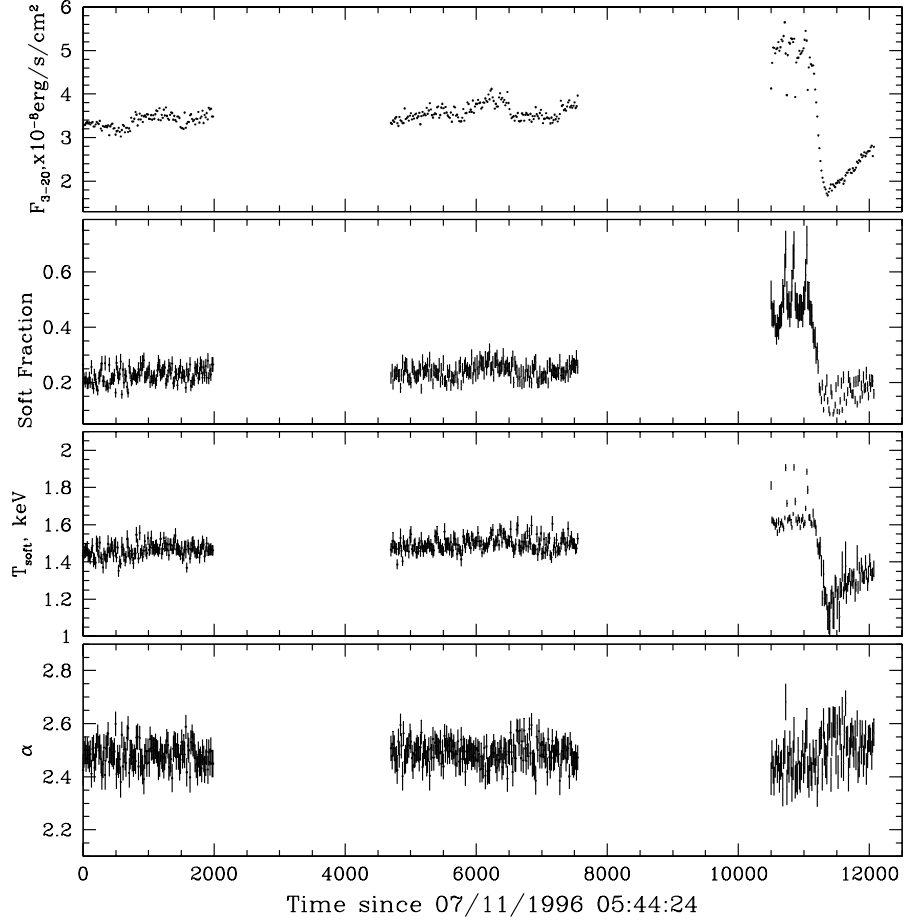


Figure 3: The evolution of the GRS 1915+105 spectral parameters for the November 7, 1996 observation (multicolor disk black body model plus power law approximation, the equivalent hydrogen column density was fixed at the value of  $5 \times 10^{22} \text{ cm}^{-2}$ ) (3 – 20 keV energy range, PCA data). 'Soft fraction' denotes the ratio of the soft component luminosity to the total luminosity in the 3 – 20 keV energy range. Each point corresponds to the 16 s integration time.

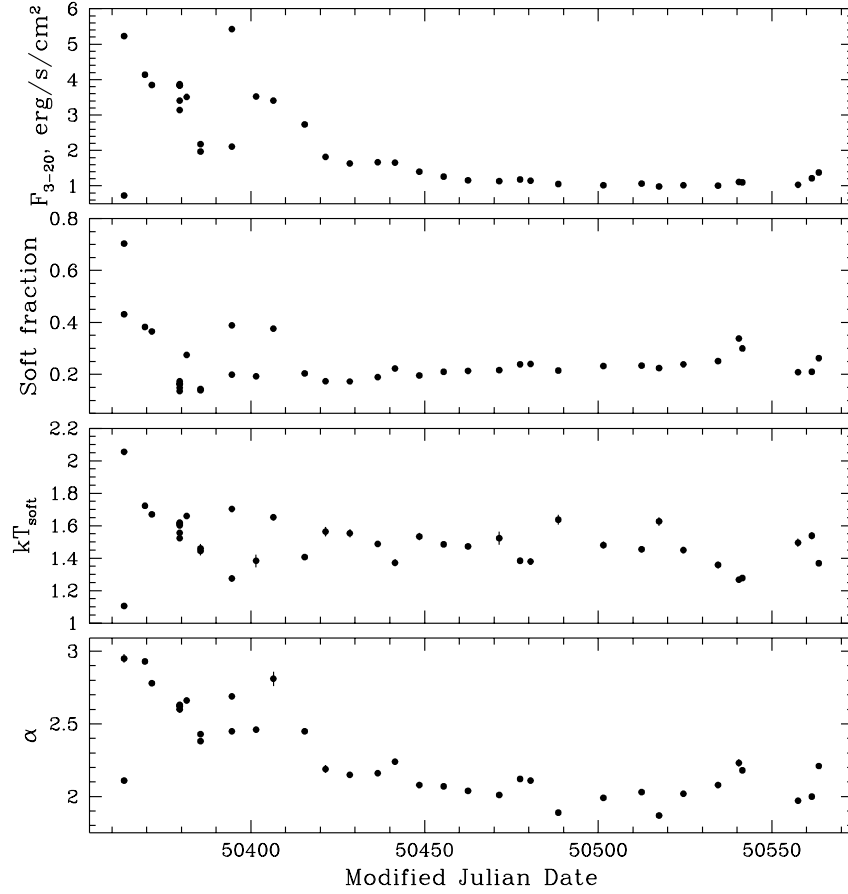


Figure 4: Evolution of the GRS 1915+105 spectral parameters (multicolor disk black body model plus power law approximation)(3 – 20 keV energy range, PCA data). 'Soft fraction' denotes the ratio of the soft component luminosity to the total luminosity in the 3 – 20 keV energy range. (*Note: for MJD 50363, 50369, 50371, 50381, 50406 observations characterized by a high level of variability the results of fitting presented by several points corresponding to the different levels of source luminosity*).



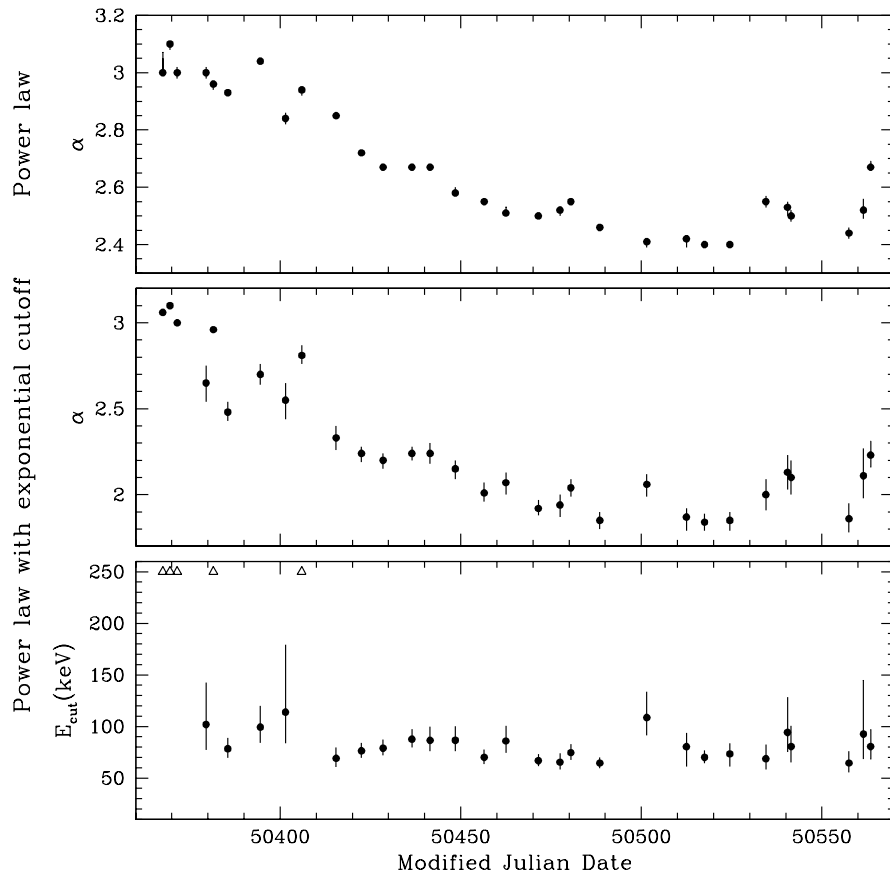


Figure 5: The evolution of the hard X-ray spectral parameters (*upper panel* – power law model approximation; *middle and bottom panel* – approximation by power law with exponential cutoff) of GRS 1915+105 during its low luminosity state and state transitions in 1996/1997 (20–150 keV energy band, HEXTE data). Note: open triangles (*bottom panel*) show HEXTE upper energy boundary (250 keV) in the cases when the high energy cutoff is not detectable within HEXTE energy range

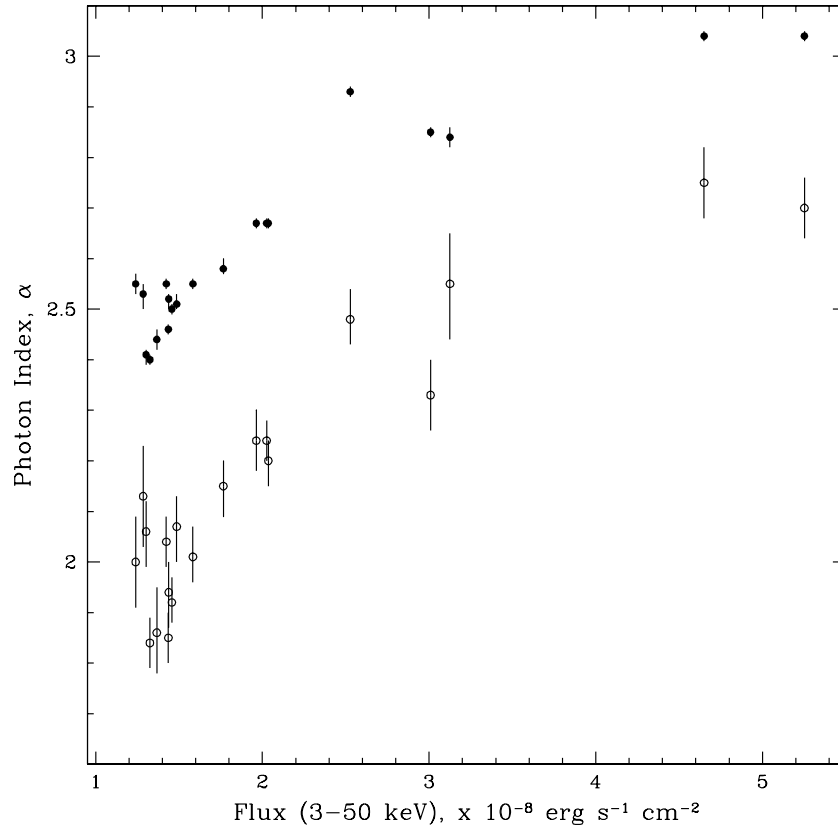


Figure 6: The slope of the high energy part of GRS 1915+105 spectrum (simple power law approximation – *solid circles*; approximation by power law with exponential cutoff – *hollow circles*) vs. 3 – 50 keV luminosity of the source (PCA and HEXTE data)

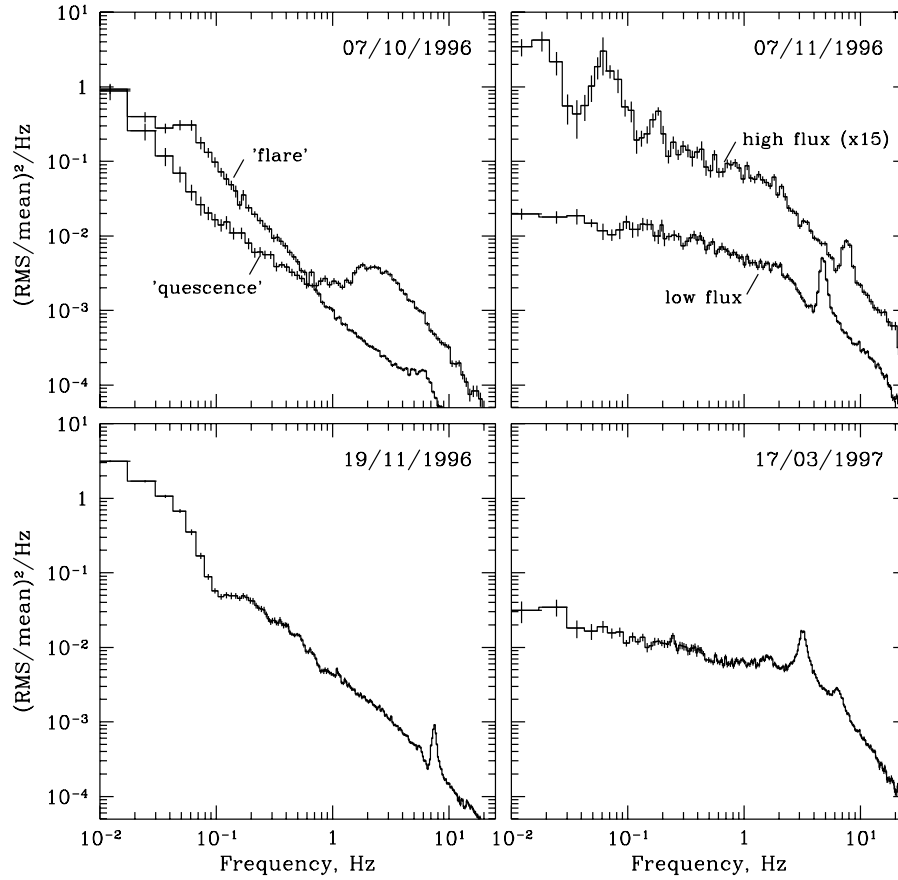


Figure 7: Typical power density spectra of GRS 1915+105 during low luminosity state and state transitions: *left upper panel* – during *high* 'flaring' state; *right upper panel* – transition (when the contribution of the soft spectral component was relatively small); *left lower panel* – transition (when the contribution of the soft spectral component is sufficiently higher); *right lower panel* – nominal low luminosity state.

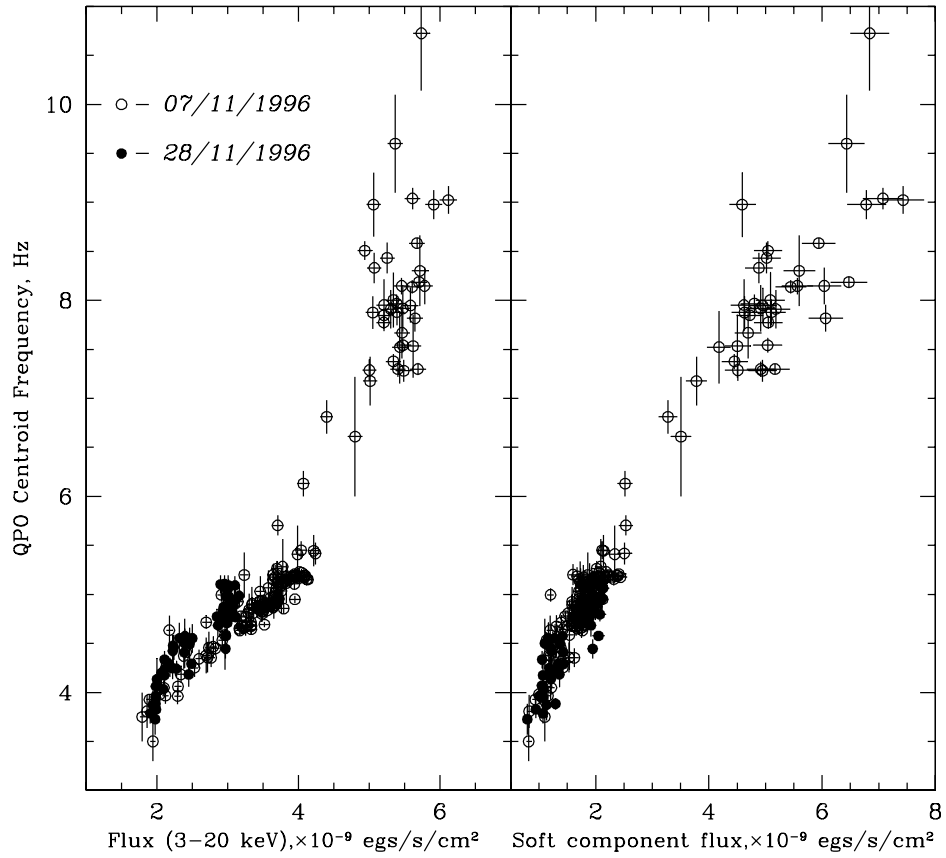


Figure 8: The evolution of the QPO centroid frequency in GRS 1915+105 power density spectrum on the source 3 – 20 keV flux (corrected for the interstellar absorption) and a bolometric flux of the soft spectral component during November 7 (*open circles*) and November 28, 1996 (*solid circles*) *RXTE* pointed observations. (Each point represents the data averaged over 16 – 48 s time intervals; PCA data).

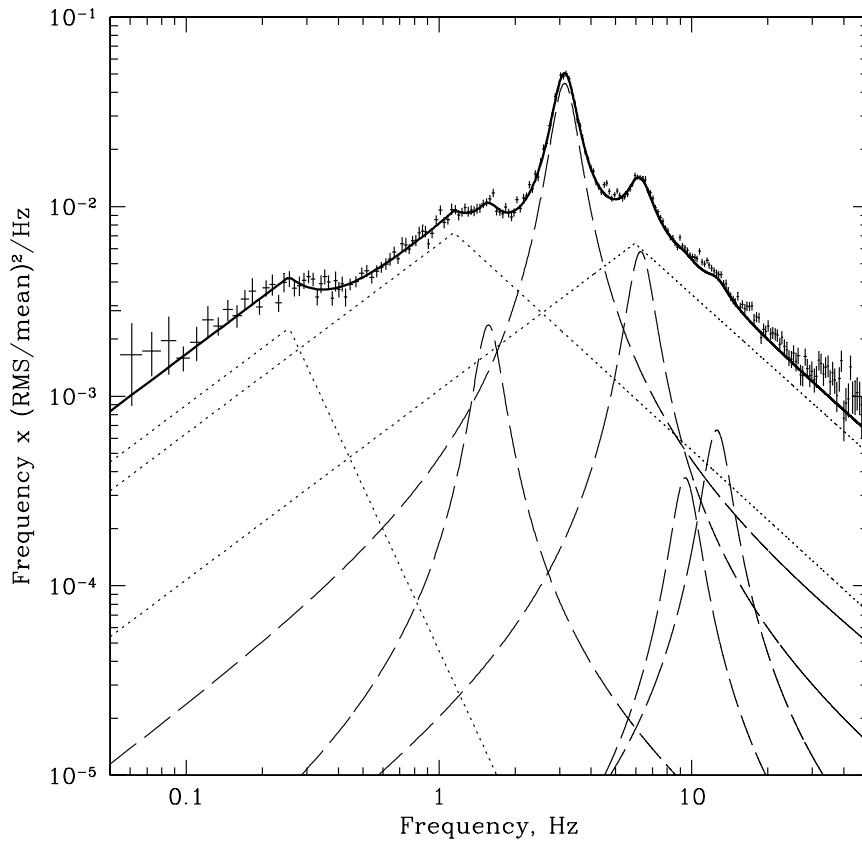


Figure 9: Schematic presentation of the model used for the approximation of the broad-band power density spectra during the low luminosity state and state transitions (*thick solid line*). The contributions of band limited noise (BLN) components, Lorentzian components are shown by *dotted lines* and *long-dashed lines* respectively. The data for the Dec. 19, 1996 observation are shown for the comparison (PCA data, 2 – 13 keV energy range).

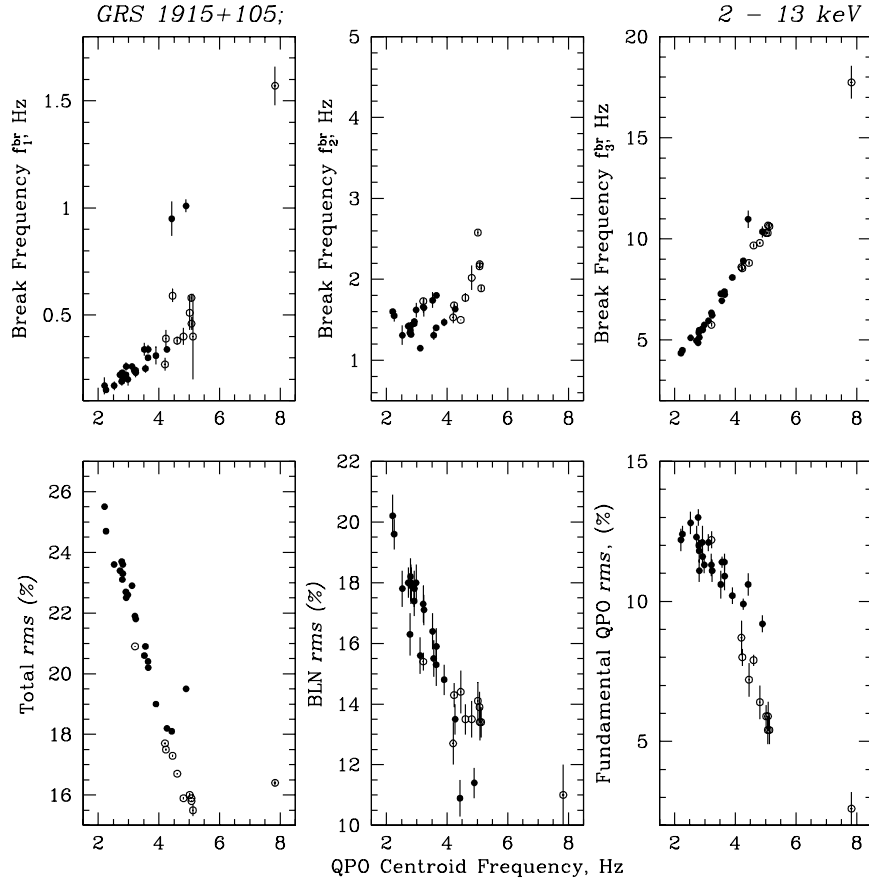


Figure 10: Main best-fit parameters of the source power density spectrum (see Tables 3, 4, 5, 6) as a functions of the fundamental QPO peak frequency (2–13 keV energy range). *Open circles* correspond to the observations covering the transition from the high luminosity state (HLS) to the low luminosity state (LLS) prior to Nov. 28, 1996 (MJD 50415); *solid circles* correspond to the period of LLS (Dec. 1996 – Apr. 1997).

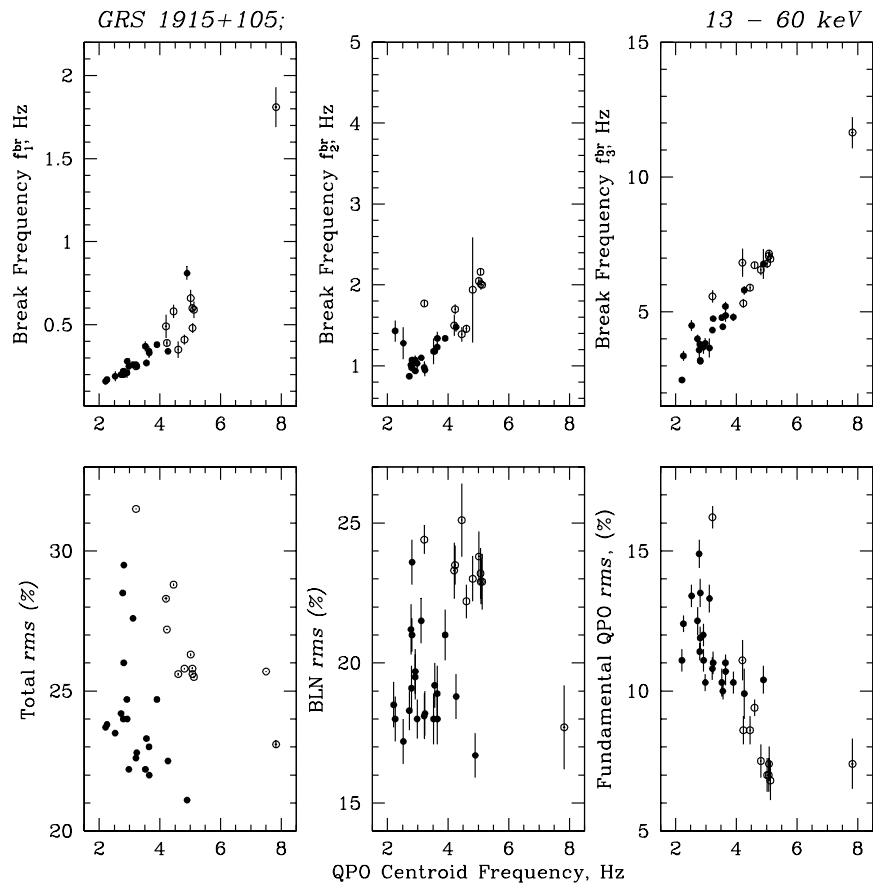


Figure 11: The same as Figure 10 but for the 13 – 60 keV energy band.

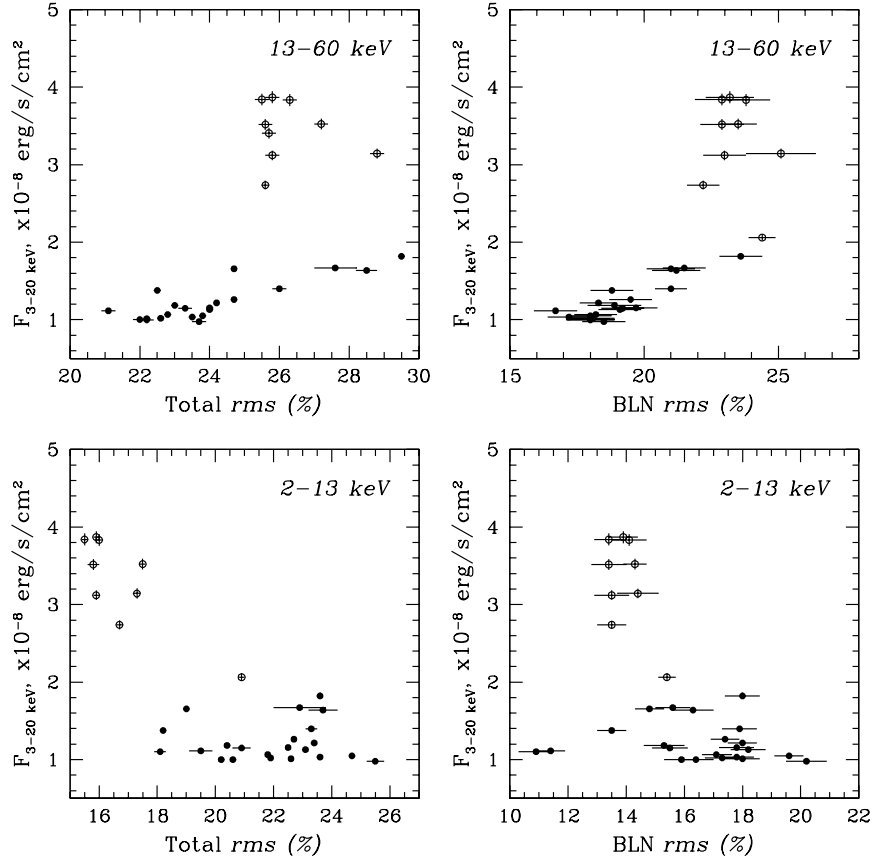


Figure 12: Total fractional *rms* and band-limited component *rms* in the 2 – 13 keV and 13 – 60 keV energy intervals integrated 0.05 – 50 Hz frequency range vs. total 3 – 20 keV X-ray flux. *Open circles* correspond to the observations covering the transition from the high luminosity state (HLS) to the low luminosity state (LLS) prior to Nov. 28, 1996 (MJD 50415); *solid circles* correspond to the period of LLS (Dec. 1996 – Apr. 1997).



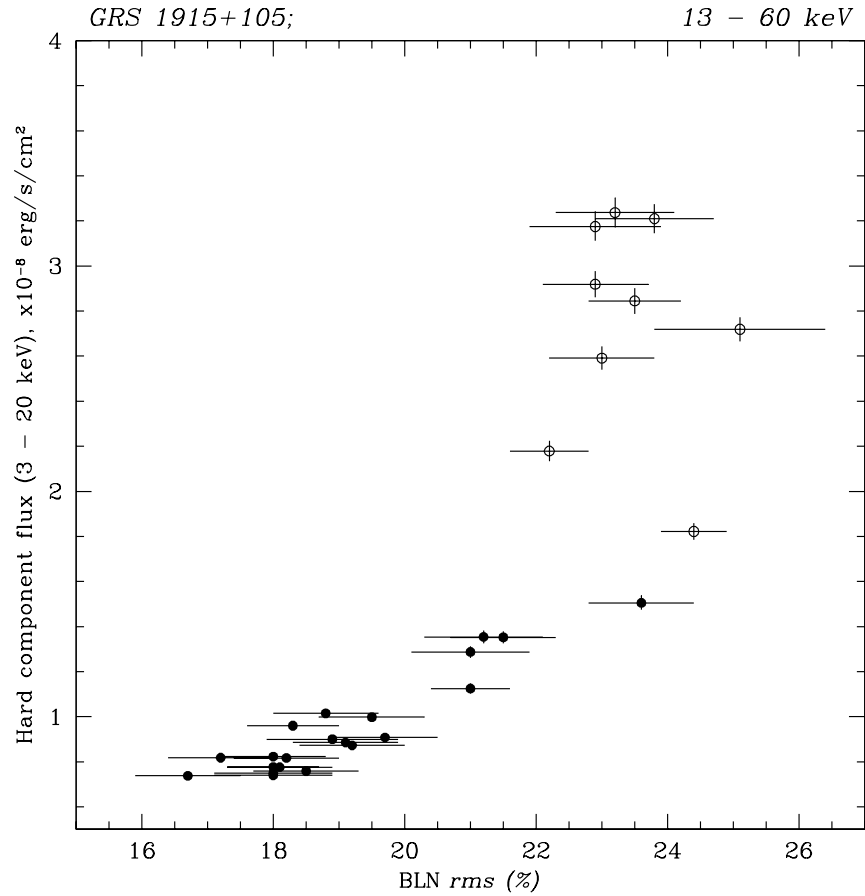


Figure 13: Total fractional *rms* and band-limited component *rms* in the 13 – 60 keV energy interval integrated 0.05 – 50 Hz frequency range vs. 3 – 20 keV hard spectral component flux. *Open circles* correspond to the observations covering the transition from the high luminosity state (HLS) to the low luminosity state (LLS) prior to Nov. 28, 1996 (MJD 50415); *solid circles* correspond to the period of LLS (Dec. 1996 – Apr. 1997).

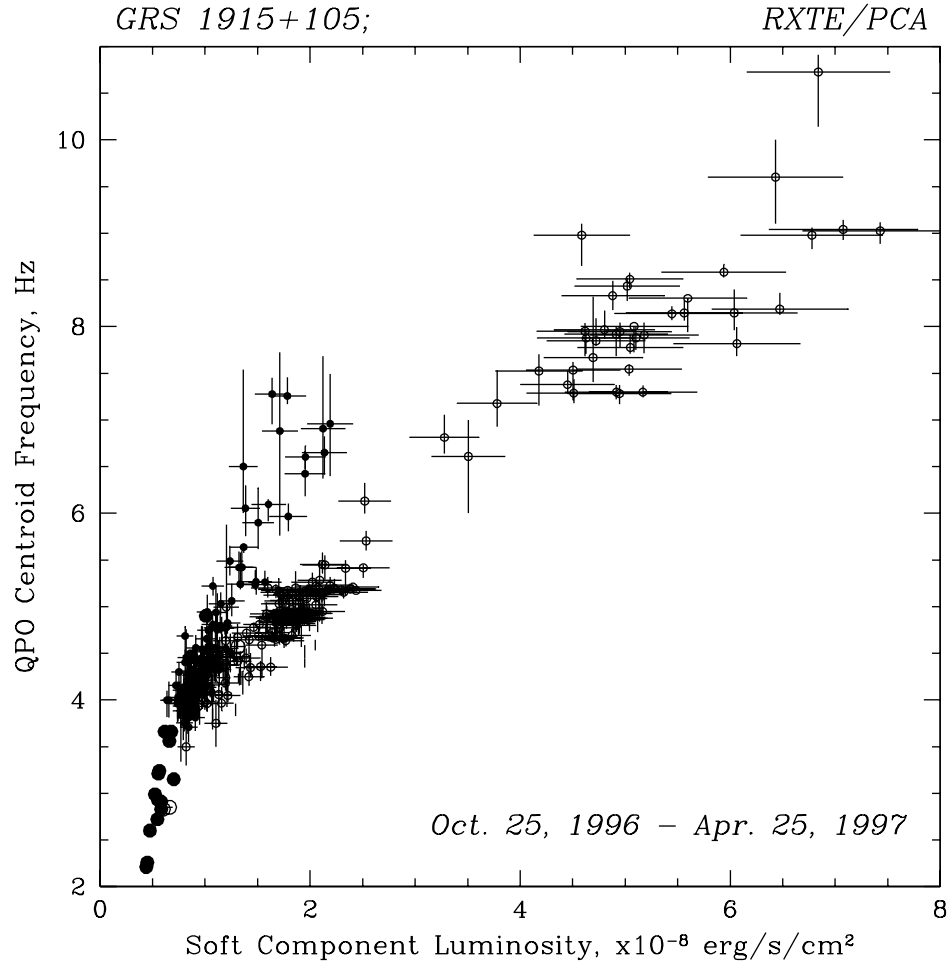


Figure 14: The dependence of the QPO centroid frequency on the estimated bolometric luminosity of the soft component obtained from the spectral fitting with our simplified model (multicolor disk black body plus power law) for the November, 1996 – April, 1997 low luminosity state and state transitions of GRS 1915+105. *Open circles* correspond to the observations, covering the period of transition from HLS to LLS prior to November 28, 1997 (MJD 50415); *filled circles* correspond to the period of low luminosity state and following rise of the source flux. *Large circles* represent the averaging over the whole observation; the results for the observations with high level of variability averaged over 32 – 80 s time intervals are presented by *small circles*.